We are IntechOpen, the world's leading publisher of Open Access books Built by scientists, for scientists

4,800
Open access books available

122,000
International authors and editors

135M
Downloads

Our authors are among the

154
Countries delivered to

TOP 1%
most cited scientists

12.2%
Contributors from top 500 universities

CLARIVATE ANALYTICS BOOK CITATION INDEX INDEXED

WEB OF SCIENCE™

Selection of our books indexed in the Book Citation Index in Web of Science™ Core Collection (BKCI)

Interested in publishing with us?
Contact book.department@intechopen.com

Numbers displayed above are based on latest data collected.
For more information visit www.intechopen.com

Chapter 4

Details of Hydraulic Jumps for Design Criteria of Hydraulic Structures

Harry Edmar Schulz, Juliana Dorn Nóbrega, André Luiz Andrade Simões, Henry Schulz and Rodrigo de Melo Porto

Additional information is available at the end of the chapter

http://dx.doi.org/10.5772/58963

1. Introduction

The sudden transition from supercritical to subcritical flow, known as hydraulic jump, is a phenomenon that, although being studied along decades, still presents aspects that need better quantification. Geometrical characteristics, such as the length of the roller (or the jump itself), still have no definitive formulation for designers of hydraulic structures. Even predictions of the sequent depths, usually made considering no shear forces, may present deviations from the observed values.

In the present chapter the geometrical characteristics of hydraulic jumps are obtained following different deductive schemes. Firstly, two adequate control volumes and the principles of conservation of mass, momentum and energy were used to obtain the length of the roller and the sequent depths. The conditions of presence or absence of bed shear forces are discussed. Secondly, two ways are used to propose the form of surface profiles: i) a "depth deficit" criterion and ii) the mass conservation principle using an "air capture" formulation. The presence or absence of inflexion points is discussed considering both formulations. Finally, the height attained by surface fluctuations (water waves and drops), useful for the design of the lateral walls that confine the jumps, is considered using empirical information and an approximation based on results of the Random Square Waves method (RSW).

Experimental data from the literature were used for comparisons with the proposed theoretical equations, allowing the adjustment of coefficients defined in these equations.

1.1. General aspects

A supercritical flow in a long horizontal channel (or having a small slope) has an inexpressive component of the weight as impulsive force. As a result, the power dissipation induces the depth of the liquid to increase along the flow, tending to its critical value. But a sudden change, a hydraulic jump, forms before the flow reaches the critical condition (which corresponds to the condition of minimum specific energy). In other words, transitions to the subcritical condition do not occur gradually in such channels. Hydraulic jumps have been studied over the years, providing a good theoretical understanding of the phenomenon, as well as experimental data that can be used to check new conceptual proposals.

The characteristics of hydraulic jumps in free flows are of interest for different applications. For example, they are used in structures designed for flow rate measurements, or for energy dissipation, like the stilling basins downstream from spillways. Although simple to produce and to control in the engineering praxis, hydraulic jumps still present aspects which are not completely understood. Interestingly, the geometrical characteristics of the jumps are among the features whose quantification still not have consensus among researchers and professionals. Perhaps the length of the jump (or the roller) is the dimension that presents the highest level of "imprecision" when quantifying it. Such difficulties may be a consequence of the simplifying hypotheses made to obtain the usual relationships. In the most known equation for the sequent depths, the shear force is neglected, and a very simple functional dependence is obtained between the depths and the Froude number (Fr). However, by neglecting the shear force, difficulties arise to calculate the length of the jump, because it does not appear in the formulation.

Many authors observed this difficulty since the beginning of the studies on hydraulic jumps. As a consequence, also a large number of solutions were presented for the sequent depths and for the length of the jump (or roller). Good reviews were presented, for example, by [1] and [2].

The hydraulic jump may be viewed as a "shock" between the supercritical and the subcritical flows. As result of this "shock", the water of the higher depth "falls down" on the water of the lower depth. Because of the main movement of the flow, and the resulting shear forces, a roller is formed in this "falling region", characterized as a two phase turbulent zone with rotating motion. This description is sketched approximately in Figure 1a. Figure 1b shows an example of this highly turbulent region, responsible for most of the energy dissipation in a hydraulic jump. Despite the fact of being turbulent (thus oscillating in time) and 3D, the hydraulic jump may be quantified as a permanent 1D flow when considering mean quantities.

Table 1 presents some studies related to the theme around the world, while Table 2 lists some academic studies in Portuguese language, developed in universities of Brazil, as a consequence of the increasing interest on hydroelectric energy in the country, and the corresponding projects of spillways with dissipation basins. The present chapter uses the background furnished by the previous studies.

http://dx.doi.org/10.5772/58963

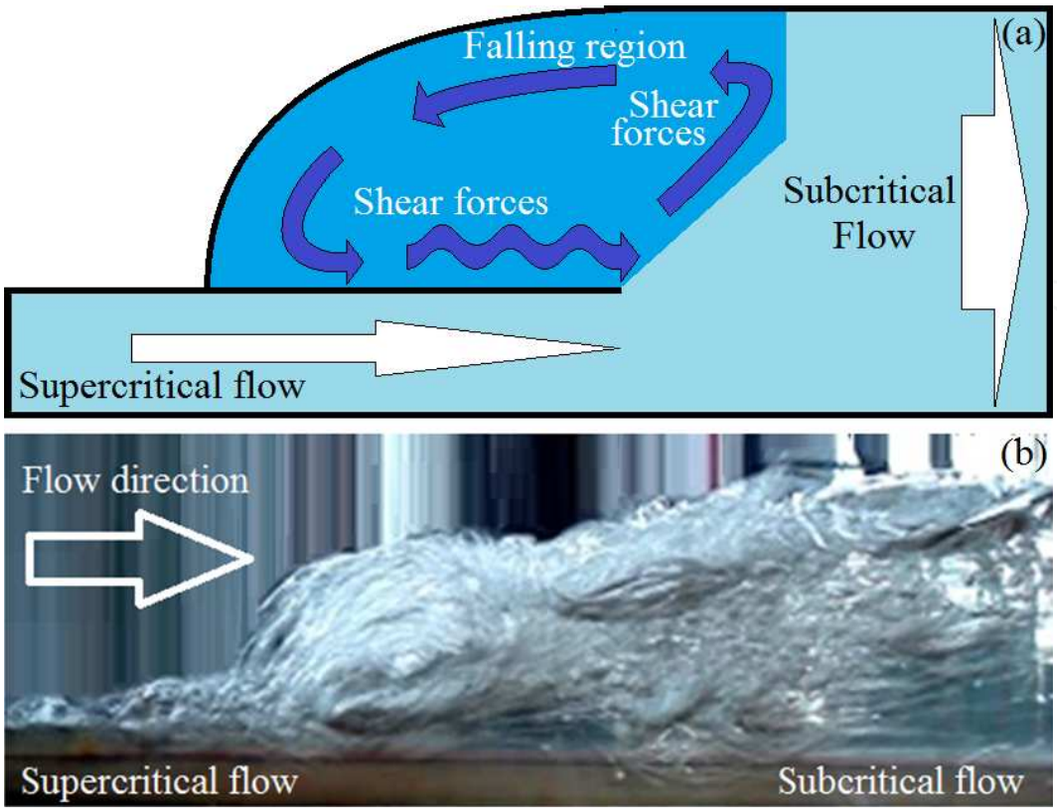

Figure 1. a) The "shock" between supercritical and subcritical flows, and the "falling region" forming the roller; b) An example of the "shock" sketched in Figure 1a.

Author (quoted by [1] and [2])	Contribution
Bidone (1818)	Experimental observations.
Belanger (1828)	Second Newtons' law applied to the jump.
Darcy & Bazin (1856/58, published 1865)	Experimental study for the evaluation of the subcritical height.
Bresse (1860)	Second Newtons' law applied to the jump.
Unwin (1880)	Second Newtons' law applied to the jump.
Feriday (1894)	Experimental study.
Merriman (1903)	Second Newtons' law applied to the jump.
Gibson (1913)	Verifying the Newtons' law.
Kennison (1916)	Second Newtons' law applied to the jump.
Riegel & Beebe (1917)	Description of the phenomenon. Verifying the Newtons' law. Discussion of the length of the jump.
Safranez (1927, 1929)	Verifying Newtons' law. Discussion of the length of the jump.
Knapp (1932)	Length of the jump.
Pietrkowski (1932)	Length of the jump.
Trahern (1932)	Localization of the jump.
Inglis & Joglekar (1933)	Second Newtons' law applied to the jump.

Author (quoted by [1] and [2])	Contribution
Einwachter (1933)	Length of the jump.
Ludin & Barnes (1934)	Length of the jump.
Woycieki (1934)	Length of the jump.
Smetana (1934)	Length of the jump.
Douma (1934)	Length of the jump.
Aravin (1935)	Length of the jump.
Kinney (1935)	Experiments and Length of the jump.
Page (1935)	Length of the jump.
Chertoussov (1935)	Length of the jump.
Bakhmeteff & Matzke (1936)	Extensive project for the generalization of equations.
Ivanchenko (1936)	Length of the jump.
Willes (1937)	Length of the jump and air entrainment.
Goodrum & Dubrow (1941)	Influence of surface tension and viscosity.
Posey (1941)	Length of the jump.
Wu (1949)	Length of the jump.
Bureau of Reclamation (1954)	Experimental study.
Schröder (1963)	Length of the jump.
Rajaratnam (1965)	Length of the jump.
Malik (1972)	Length of the jump.
Sarma & Newnham (1973)	Length of the jump.
Hager *et al*. (1990) [2]	Length of the roller.

Table 1. Studies related to hydraulic jumps. Table considering information contained in the studies of [1] and [2].

Having so many proposals, it may be asked why is there no consensus around one of the possible ways to calculate the geometrical characteristics. A probable answer could be that different solutions were obtained by detailing differently some of the aspects of the problem. But perhaps the most convincing answer is that the presented mechanistic schemes are still not fully convincing. So, it does not seem to be a question about the correctness of the used concepts, but on how they are used to obtain solutions. In other words, it seems that there are still no definitive criteria, generally accepted.

This chapter shows firstly the traditional quantification of the sequent depths of hydraulic jumps, which does not consider the bed shear force. In the sequence, using two adequate control volumes and the principles of conservation of mass, momentum and energy, an equation for the length of the roller is furnished. Further, the sequent depths are calculated considering the presence and the absence of bed shear forces, showing that both situations lead to different equations. Still further, the surface profiles and the height attained by the surface fluctuations (drops and waves) are discussed, and equations are furnished using i) a "depth deficit" criterion, ii) the mass conservation principle using an "air capture" formula-

tion, and iii) an approximation that uses results of the Random Square Waves method (RSW). Literature data are used to quantify coefficients of the equations and to compare measured and calculated results.

Author	Advisor	Nature of study	University
Jayme Pinto Ortiz (1982) [3]	Milton Spencer Veras Jr.	MSc Dissertation	USP*
Jayme Pinto Ortiz (1989) [4]	Angelo Raffaele Cuomo	Dr Thesis	USP
Margarita M. Lopez Gil (1991) [5]	Kokei Uehara	MSc Dissertation	USP
Yosuke Yamashiki (1994) [6]	Podalyro Amaral de Souza	MSc Dissertation	USP
Jaime Frederici Gomes (2000) [7]	Marcelo Giulian Marques	MSc Dissertation	UFRGS**
Edgar F. Trierweiler Neto (2006) [8]	Marcelo Giulian Marques	MSc Dissertation	UFRGS
Rafael André Wiest (2008) [9]	Marcelo Giulian Marques	MSc Dissertation	UFRGS
Alexandre A. Mees Alves (2008) [10]	Marcelo Giulian Marques	MSc Dissertation	UFRGS
Daniela Müller de Quevedo (2008) [11]	Robin Thomas Clarke	Dr Thesis	UFRGS
Simone Maffini Cerezer (2008) [12]	Robin Thomas Clarke	Dr Thesis	UFRGS
Eder Daniel Teixeira (2008) [13]	Marcelo Giulian Marques	Dr Thesis	UFRGS
Jayme Pinto Ortiz (2011) [14]	-	Assoc. Prof. Thesis	USP
Maurício Dai Prá (2011) [15]	Marcelo Giulian Marques	Dr Thesis	UFRGS
Pedro E. de A. e Souza (2012) [16]	Marcelo Giulian Marques	MSc Dissertation	UFRGS
Juliana Dorn Nóbrega (2014) [17]	Harry Edmar Schulz	MSc Dissertation	USP

Table 2. Academic studies conducted in Brazil about hydraulic jumps. *USP: University of São Paulo; **UFRGS: Federal University of Rio Grande do Sul.

1.2. Traditional quantification of sequent depths

The Newton's second law for a closed system establishes that:

$$\sum \vec{F} = d\left(m\vec{V}\right)/dt\,|_S \tag{1}$$

where $\vec{F}$ is the force, m is the mass of the system, $\vec{V}$ is the speed, and t is the time. The system is indicated by the index S. Considering the Euler formulation, for open systems or control volumes, equation (1) is rewritten using the Reynolds transport theorem, furnishing:

$$\sum \vec{F} = \frac{d}{dt}\iiint_{VC} \vec{V}\rho dVol + \oiint_{SC} \vec{V}\left(\rho\vec{V}\cdot\vec{n}dA\right) \tag{2}$$

where ρ is the density, $\vec{n}$ is the unit vector normal to the control surface and pointing outside of the control volume, and A is the area of the control surface.

Hydraulic jumps in horizontal or nearly horizontal channels are usually quantified using a control volume as shown in Figure 2, with inlet section 1 and outlet section 2, no relevant shear

forces at the bottom and the upper surface (F_{shear}), no effects of the weight (W_x), and hydrostatic pressure distributions at sections 1 and 2.

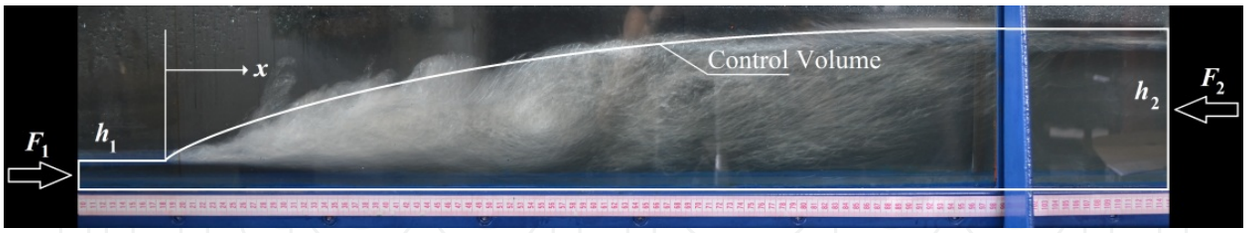

Figure 2. Hydraulic jump and adopted control volume. The photograph was taken to show the air bubbles ascending, and the outlet section located where no air bubbles are present.

For steady state conditions, equation (2) is written as:

$$\left\{F_1 - F_2 + W_x - F_{shear} \cong F_1 - F_2 =\right\} \quad \sum \vec{F} = \iint_{SC} \vec{V}\left(\rho \vec{V} \cdot \vec{n} dA\right) \quad \left\{= \rho\left(V_2^2 A_2 - V_1^2 A_1\right)\right\} \tag{3}$$

In the sequence, from $Q=V_1A_1=V_2A_2$:

$$F_1 - F_2 = \rho Q^2 \left(\frac{1}{A_2} - \frac{1}{A_1}\right) \tag{4}$$

Q is the water flow rate, ρ is the water density, F_1 and F_2 are the forces due to the pressure at the inlet and outlet sections, respectively. The hydrostatic distribution of pressure leads to:

$$F_1 = \rho g h_1 A_1 / 2 \qquad \text{and} \qquad F_2 = \rho g h_2 A_2 / 2 \tag{5}$$

g is the acceleration of the gravity, h_1 and h_2 are the water depths, and A_1 and A_2 are the areas of the cross sections 1 and 2, respectively. Substituting equations (5) into equation (4) produces:

$$Q^2 / gA_1 + A_1 h_1 / 2 = Q^2 / gA_2 + A_2 h_2 / 2 \tag{6}$$

For a rectangular channel $A_1=Bh_1$, $A_2=Bh_2$, where B is the width of the channel. Further, the definition $q=Q/B$ is of current use. Algebraic steps applied to equation (6) lead to:

$$h_1^2 - h_2^2 = \frac{2q^2}{g}\left(\frac{1}{h_2} - \frac{1}{h_1}\right) \Rightarrow (h_2 - h_1)(h_2 + h_1) = \frac{2q^2}{g}\left(\frac{1}{h_2} - \frac{1}{h_1}\right) \Rightarrow (h_2 + h_1) = \frac{2q^2}{g h_1 h_2} \Rightarrow$$

$$\Rightarrow h_1^2 h_2 + h_2^2 h_1 = \frac{2q^2}{g} \Rightarrow \frac{h_2^2}{h_1^2} + \frac{h_2}{h_1} - \frac{2q^2}{g h_1^3} = 0 \quad \text{or} \quad \left(\frac{h_2}{h_1}\right)^2 + \frac{h_2}{h_1} - 2Fr_1^2 = 0$$

http://dx.doi.org/10.5772/58963

Solving the final obtained equation for h_2/h_1, the result is:

$$h^{\#} = h_2 / h_1 = \left(\sqrt{8Fr_1^2 + 1} - 1\right) / 2 \quad \text{where} \quad Fr_1 = V_1 / \sqrt{gh_1} \tag{7}$$

Figure 3 shows that equation (7) compares well with experimental results.

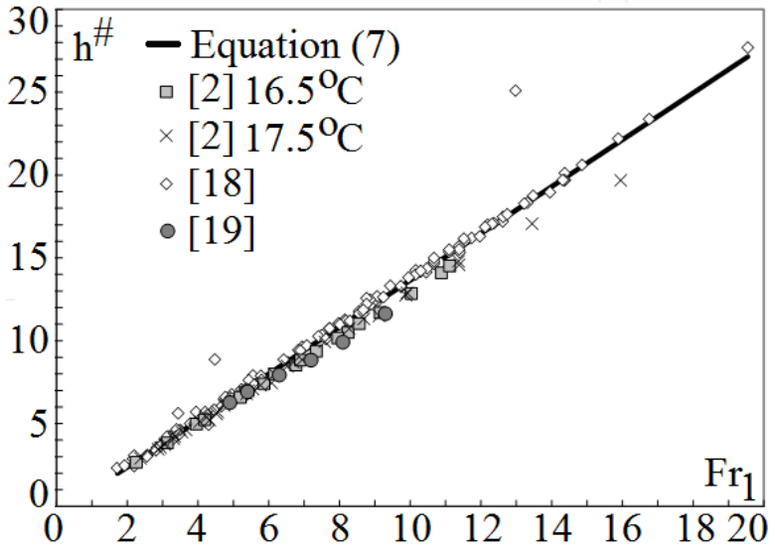

Figure 3. Sequent depths ratio as a function of the Froude number. Data of [2, 18, 19].

The experimental data of [2] and [19] show that predictions of equation (7) may generate relative errors in the range of 0.10% to 12.2%. Considering simpler equations, different proposals may be found in the literature. For example. for Fr_1>2 [20] suggests the simplified form $h^{\#}=\sqrt{2}Fr_1-1/2$, (where $h^{\#}=h_2/h_1$). But other linear equations are also suggested. Equation (8), for example, is valid for 2.26<Fr_1<15.96, has a correlation coefficient of 0.99, maximum relative error of 5.4%, for the data of Figure 3, excluding [18].

$$h^{\#} = 1.29Fr_1 - 0.116 \tag{8}$$

Although alternative equations exist in the literature, equation (7) is one of the most known and accepted conclusions for hydraulic jumps. Interestingly, hydraulic jumps are used as dissipative singularities, but their most known design equation implies absence of dissipative shear forces. This contradiction is one of the reasons of the continuing discussion on the theme. In this chapter we present (see items 2.1.1, 2.1.2, 2.1.3) a way to conciliate the dissipative characteristic of the jump and the adequacy of the predictions given by equation (7).

1.3. Equations of the literature for the lengths of the roller and the hydraulic jump

The experimental determination of the length of the hydraulic jump is not a simple task. The intense turbulence and the occurrence of single-phase and two-phase flows adds difficulties to the measurement of flow depths, velocity fields, pressure distributions and the lengths of the roller and the hydraulic jump. A further difficulty is related to the definition of the end of the hydraulic jump. Accordingly to [1], the earliest formulation for the length of the hydraulic jump was proposed by, Riegel and Beebe, in 1917, while [2] suggest that the first systematic study of the length of the roller was made by Safranez, in 1927-1929. [21] defined the end of the hydraulic jump as the position where the free surface attains its maximum height, and the upper point of the expanding main flow (located between the roller and the bottom of the channel) coincides with the surface, beginning to decline towards the subsequent gradually varied flow. This definition led to lengths greater than the rollers.

[2] mention Schröder, who in 1963 used visualizations of the free surface to quantify jump lengths. However, such visual procedures depend on personal decisions about different aspects of the moving and undulating surface. [2] also cite Malik, who in 1972 employed a probe to measure forces and to locate the superficial region with zero mean force. The position of this region corresponds to the roller length, and the experimental error was about 8%.

The results of [18] are among the most used for calculating lengths of hydraulic jump stilling basins, downstream of spillways. The end of the jump was assumed as the position where the high velocity jet starts to peel off the bottom, or the section immediately downstream of the roller.

[19] measured pressure distributions along the bottom of a horizontal channel for hydraulic jumps with Fr_1 between 4.9 and 9.3. The pressure records were used to calculate coefficients of skewness and kurtosis of the measured data along the channel. The authors obtained values of coefficients of kurtosis around 3.0, which became practically constant for distances greater than $x/(h_2\text{-}h_1)$=8.5. The authors then defined the end of the hydraulic jump as L_j=8.5(h_2-h_1).

[22, 23] measured water depths along a hydraulic jump in a rectangular channel, for Fr_1=3.0, using an ultrasonic sensor to locate the water surface. The sensor was moved along the longitudinal axis of the channel. Vertical turbulent intensities and related Strouhal numbers were calculated for each measurement position. The authors suggested to estimate the length of the jump using the final decay of the vertical turbulent intensity at the free surface, obtaining L_j=9.5(h_2-h_1). Similarly, [24, 25] and [17] generated and analyzed data of ultrasonic sensors and high speed cameras to evaluate comparatively the results of the sensors and to better locate the surface.

Some equations for the length of the hydraulic jump and the roller are resumed in Table 3. Most of them can be written as L_j/h_2=f(Fr_1) when using equation (7). A qualitative comparison between some of these equations is shown in Figure 4, assuming the interval $2 \leq Fr_1 \leq 20$ as valid for all equations.

Riegel and Beebe (1917):	$L_j \approx 5\left(h_2 - h_1\right)$	(9)
Safranez (1927):	$L_j \approx 5.2h_2$	(10)
Ludin and Barnes (1934):	$L_j = \left(4.5 - V_1 / V_c\right)h_2$	(11)
Woycieki (1934):	$L_j = \left(h_2 - h_1\right)\left(8 - 0.05h^{\#}\right)$	(12)
Smetana (1934):	$L_j \approx 6\left(h_2 - h_1\right)$	(13)
Douma (1934):	$L_j = 5.2h_2$	(14)
Aravin (1935):	$L_j \approx 5.4\left(h_2 - h_1\right)$	(15)
Kinney (1935):	$L_j = 6.02\left(h_2 - h_1\right)$	(16)
Page (1935):	$L_j = 5.6h_2$	(17)
Chertoussov(1935):	$L_j = 10.3h_1\left(Fr_1 - 1\right)^{0.81}$	(18)
Bakhmetef, Matzke(1936):	$L_j = 5\left(h_2 - h_1\right)$	(19)
Ivanchenko (1936):	$L_j = 10.6\left(h_2 - h_1\right)\left(Fr_1^2\right)^{-0.185}$	(20)
Posey (1941):	$L_j \approx 4.5 - 7\left(h_2 - h_1\right)$	(21)
Wu (1949):	$L_j = 10\left(h_2 - h_1\right)Fr_1^{-0.16}$	(22)
Hager *et al*.(1992) [20]:	$L_j / h_1 = 220tgh\left[\left(Fr_1 - 1\right)\right]$	(23)
Hager *et al*. (1990) [2]:	$L_r / h_1 = 12 + 8a_r tgh\left(Fr_1 / a_r\right)^{\$}$	(24)
Marques *et al.* (1997) [19]:	$L_j = 8.5\left(h_2 - h_1\right)$	(25)
Simões *et al.* (2012) [23]:	$L_j = 9.52\left(h_2 - h_1\right)$	(26)
Knapp (1932):	$L_j = \left(62.5h_1 / E_1 + 11.3\right)\left[\left(V_1 - V_2\right)^2 / \left(2g\right) - \left(E_1 - E_2\right)\right]$	(27)
Einwachter (1933):	$L_r = \left(15.2 - 0.24h^{\#}\right)[\left(h^{\#} - 1\right) - V_1^2\left(h^{\#} - 1\right) / \left(h^{\#}2g\right)$	(28)
Simões (2008) [26]:	$L_j / h_2 = \left(Fr_1^2 - 81.85Fr_1 + 61.13\right) / \left(-0.62 - 10.71Fr_1\right)$	(29)

Table 3. Equations for the length of the roller and the hydraulic jump. The table uses citations of [1, 2, 18]. V_c=critical velocity; E=specific energy. $^{\$}\alpha_r$=20 if h_1/B<0.1; α_r=12,5 if 0.1≤h_1/B≤0.7. B=channel width. If Fr_1<6, following approximation may eventually be used: L_r/h_1=8Fr_1-12.

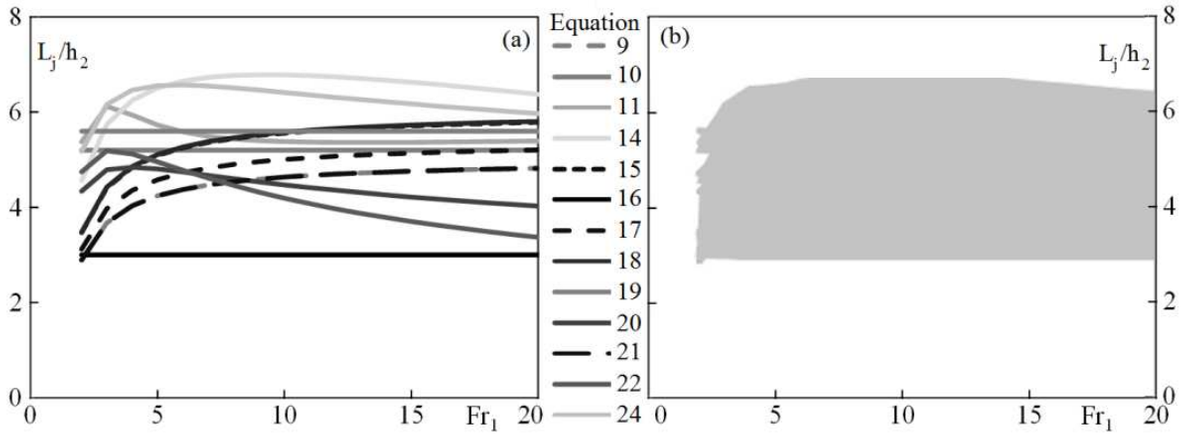

Figure 4. a) Comparison of equations of nondimensional jump lengths proposed by different authors cited in Table 3, as a function of Fr_1; b) The region of the graph covered by the equations.

Experimental data of [18] for L_j/h_2, conducted for Fr_1 between about 2 and 20, are shown in Figure 5. The middle curve corresponds to the adjusted equation (29) proposed by [26].

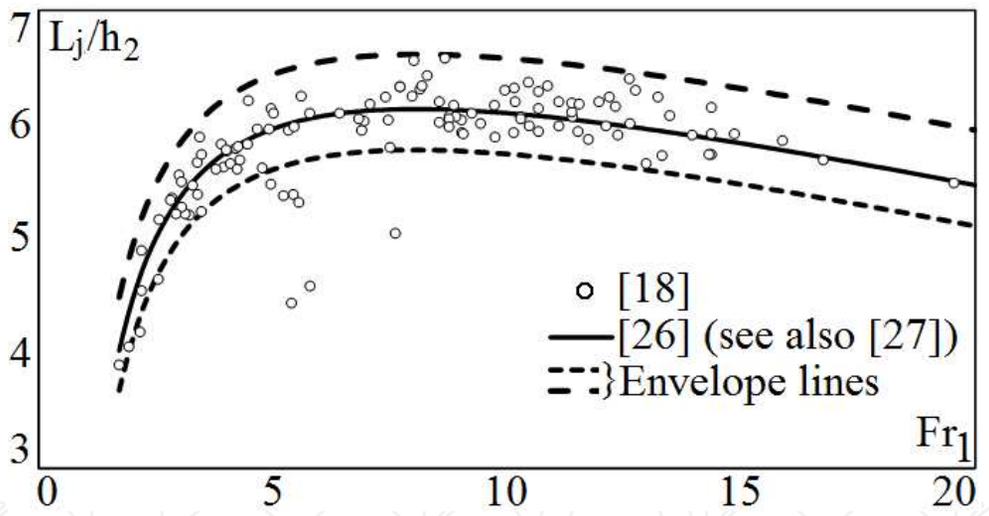

Figure 5. Data of L_j/h_2 obtained by [18], and equation (29) presented by[26] (see also [27]). The upper and lower curves are shown as envelopes.

2. Proposed formulation

2.1. The criterion of two control volumes

The focus of this item is to present the equations obtained for the length of the roller and for the sequent depths using only one deduction schema. A detailed explanation of the forces that maintain the equilibrium of the expansion is presented firstly, followed by their use to quantify

http://dx.doi.org/10.5772/58963

the power dissipation. The integral analysis is used for the two control volumes shown in Figure 6.

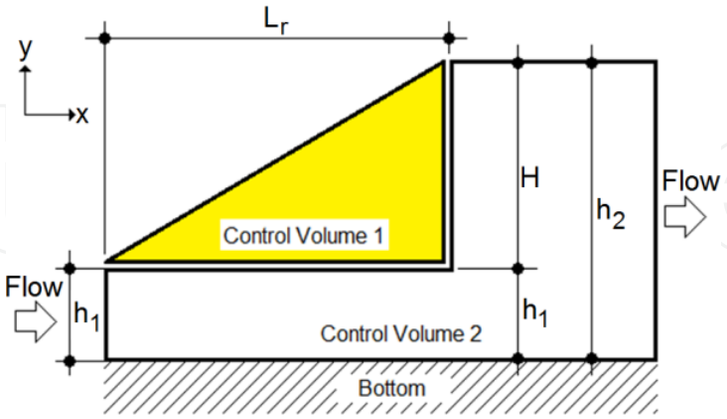

Figure 6. The two control volumes used in the present formulation, for the quantification of the length of the roller and the sequent depths of the hydraulic jump.

The two control volumes allow considering details, such as the vortex movement of the roller and the recirculating flow rate. The regime of the flow is permanent (stationary conditions), and both control volumes are at rest. In order to simplify the calculations, control volume 1 (CV1) contains the roller of the jump and ideally does not exchange mass with control volume 2 (CV2). But, as a result of the shear forces at the interface between both volumes, they exchange momentum and energy. The analyses of the flows in both volumes are made here separately.

2.1.1. Length of the roller using control volume 1 (CV1)

i. Global Analysis of CV1

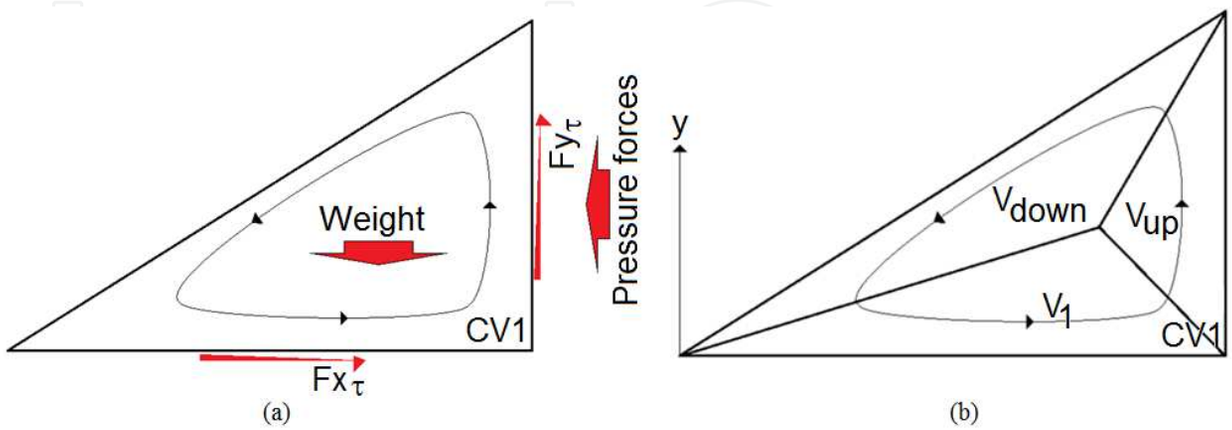

Figure 7. a) CV1 and the forces acting on it. $F_{x\tau}$ and $F_{y\tau}$ are shear forces acting in the x and y directions, respectively; b) The three regions of influence of the characteristic velocities (V_1, V_{up}, and V_{down}) defined for CV1.

Figure 7a shows CV1 already isolated from CV2. Because there is no mass exchange between CV1 and the main flow (CV2), the mass conservation equation (30) reduces to the elementary form (31):

$$\frac{d}{dt}\iiint_{CV1}\rho dVol + \oiint_{CS}\rho\vec{V}.d\vec{A} = 0 \tag{30}$$

$$\frac{dM}{dt} = 0 \tag{31}$$

CS is the control surface and *M* is the mass in CV1. For the momentum conservation, the general integral equation also reduces to the simplest form:

$$\vec{F} = \frac{d}{dt}\iiint_{CV1}V\rho dVol + \oiint_{CS}\vec{V}\rho\vec{V}.d\vec{A} = 0 \tag{32}$$

Because there are no mass fluxes across the surfaces, and the flow is stationary, the resultant of the forces must vanish. It implies that, for the coordinate directions *x* and *y*:

$$F_x = 0 \qquad \text{and} \qquad F_y = 0 \tag{33}$$

The mass in CV1 is constant and the volume does not change its form (that is, it will not slump and flow away). It implies that the shear forces of the flow must equate the pressure forces in the *x* direction, and the weight in the *y* direction. So, from Figure 7a, and equations (33) it follows that:

$$F_{x\tau} = \frac{\rho g H^2 B}{2} \tag{34}$$

$$F_{y\tau} = \frac{\rho g L_r B H}{2}\theta_1 \tag{35}$$

θ_1 is a constant that corrects the effects of using the inclined straight line instead of the real form of the water surface (understood as the water equivalent depth). $H=h_2-h_1$ and L_r is the length of the roller.

The shear forces presented in Figure 7a induce movement to the water in CV1, so that, in a first step, power is inserted into CV1. No mass exchanges occur across the control surface, and this energy is converted into thermal energy in CV1. But, further, this thermal energy is lost

http://dx.doi.org/10.5772/58963

to the environment (main flow and atmosphere), so that the equilibrium or the stationary situation is maintained, and the energy inserted into the volume is released as heat to the environment.

Considering the energy equation, for stationary conditions and no mass exchange between the control volumes, it follows that:

$$\dot{Q}-\dot{W}=\frac{d}{dt}\iiint_{CV1} e\rho dVol+\oiint_{CS}(e+\frac{p}{\rho})\rho\vec{V}.d\vec{A}=0 \qquad \text{where} \qquad e=\frac{V^2}{2}+gy+u \tag{36}$$

$\dot{W}$ and $\dot{Q}$ are the work and the thermal energy exchanged with the surroundings per unit time, u is the specific internal energy and y is shown in Figure 7b. The surface integral vanishes because there is no mass flow across the control surface. From the first member of equation (36) it follows that:

$$\dot{W}=\dot{Q}=Power\ loss \tag{37}$$

Equation (37) means that, in this stationary case, all power furnished to CV1 is lost as heat. Equations (34, 35) and (37) allow writing:

$$\frac{\rho g H^2 B V_1}{2}+\frac{\rho g LB H}{2}\left(\frac{H}{\Delta t_y}\right)_{up}\theta_1=Power\ loss \tag{38}$$

$(H/\Delta t_y)$ is the mean vertical velocity (V_{up} in Figure 7b) that allows calculating the power furnished by the upwards force. Δt_y is the mean travel time of the water in the vertical direction (positive y axis, see Figure 7b). The mean upwards flow rate equals the mean downwards flow rate (because no mass is lost in CV1), so that, considering mean quantities for the involved areas, it follows that:

$$Area_{up}\left(\frac{H}{\Delta t_y}\right)_{up}=Area_{down}\left(\frac{H}{\Delta t_y}\right)_{down} \tag{39}$$

Or, because H is the same for both directions (up and down):

$$\Delta t_{y up}=\left(\frac{Area_{up}}{Area_{down}}\right)\Delta t_{y down} \tag{40}$$

Equations (31) through (40) were obtained from integral conservation principles. In order to quantify the geometrical characteristics of the hydraulic jump, the variables *Power loss*

and $\Delta t_{y_{up}}$ still need to be expressed as functions of the basic flow parameters. It is necessary, now, to consider the movement inside of the CV1, that is, to perform an intrinsic analysis in addition to the global analysis.

ii. Intrinsic Analysis of CV1

The total power loss in CV1 is the result of losses occurring in regions subjected to different characteristic velocities. Easily recognized are the velocity V_1 and the upwards velocity $H/\Delta t_{y_{up}}$. Furthermore, from equation (40) it follows that $\Delta t_{y_{up}}$ can be obtained from the downwards movement. From these considerations, three regions influenced by different "characteristic velocities" may be defined in CV1, as shown in Figure 7b. The *Power loss* of equation (38) is thus calculated as a sum of the losses in each region of Figure 7b, that is:

$$Power\ loss = \dot{W}\left(V_1\right) + \dot{W}\left(V_{up}\right) + \dot{W}\left(V_{down}\right) \tag{41}$$

The downwards region is considered firstly, following a particle of fluid moving at the "falling" boundary of the control surface, as shown in Figure 8a. (See also Figures 1a and 1b).

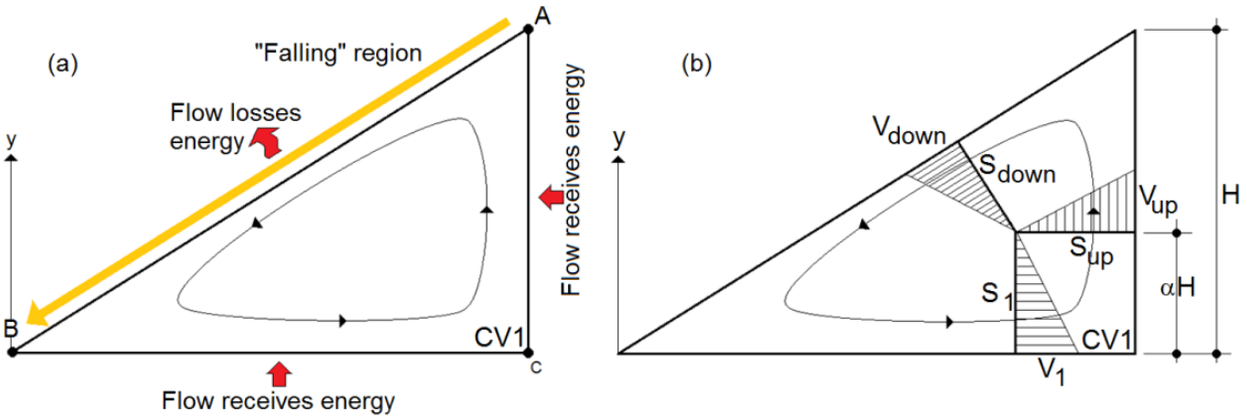

Figure 8. a) The "falling" of a particle in the "downwards region", between points A and B; b) Transversal sections S_1, S_{up}, and S_{down} in the roller.

Taking the movement along $\overline{AB}$ in Figure 8a, equation (42) applies:

$$y_A + \frac{p_A}{\rho g} + \frac{V_A^2}{2g} = y_B + \frac{p_B}{\rho g} + \frac{V_B^2}{2g} + h_{loss} \tag{42}$$

p is the pressure, which does not vary at the surface. V_A equals zero, so that the characteristic velocity is a function of V_B. Considering V_B=V_{down} and y_B=0, it follows:

http://dx.doi.org/10.5772/58963

$$H = \frac{V_{down}^2}{2g} + h_{loss} \tag{43}$$

For local dissipations h_{loss} is represented as proportional to the kinetic energy, considering a representative velocity. For the region of V_{down} (see Figures 7b and 8) it follows that:

$$h_{loss} = K\frac{V_{down}^2}{2g}, \qquad V_{down} = \sqrt{\frac{2\,g\,H}{1+K}} = \sqrt{2\,g'H}, \qquad g' = \frac{g}{1+K} \tag{44}$$

The "falling time" along $\overline{AB}$ is thus given by:

$$\Delta t_{y\,down} = \sqrt{\frac{2H}{g'}} \tag{45}$$

Equations (40) and (45) lead to:

$$\Delta t_{yup} = \left(\frac{Area_{up}}{Area_{down}}\right)\sqrt{\frac{2H}{g'}} = \theta_2\sqrt{\frac{2H}{g}} \tag{46}$$

The coefficient θ_2 accounts for the proportionality constant K of equation (44), the ratio between the mean areas of equation (40), and the use of the characteristic velocity. The power loss of the mean descending flow in the region of V_{down} is given by:

$$\dot{W}\left(V_{down}\right) = \rho g\,Q_R h_{loss} = K\rho\,Q_R\frac{V_{down}^2}{2} = \frac{K}{1+K}\rho g Q_R H \tag{47}$$

The rotating flow rate Q_R in the roller is the remaining parameter to be known. Because no variation of mass exists, it may be quantified at any position (or transversal section "S") **of the roller** (S_1, S_{up}, and S_{down}) as shown in Figure 8b. That is, Q_R=Q_1=Q_{up}=Q_{down}. Section S_1 is used here to quantify Q_R. A general equation for the velocity profile in section S_1 is used, following a power series of y, as:

$$\frac{V}{V_1} = \sum_{i=1}^{\infty}\beta_i\left(\frac{y}{\alpha H}\right)^i \tag{48}$$

αH expresses the maximum value of y in S_1, as shown in Figure 8b. β_i are coefficients of the power series, in which β_0=1. The mean velocity in section S_1 is obtained through integration, and Q_R is given by multiplying the mean velocity by the area αBH, furnishing, respectively:

$$\overline{V} = V_1 \sum_{i=1}^{\infty} \frac{\beta_i}{i+1}, \qquad Q_R = Q_1 = V_1 BH \sum_{i=1}^{\infty} \frac{\alpha\beta_i}{i+1} \tag{49}$$

Combining equations (47) and (49) results in:

$$\dot{W}\left(V_{down}\right) = \rho g V_1 B H^2 \theta_3, \qquad \theta_3 = \frac{K}{1+K} \sum_{i=1}^{\infty} \frac{\alpha\beta_i}{i+1} \tag{50}$$

Following similar steps for the flow in the region of V_1, the power consumption is given by:

$$h_{loss} = K \frac{V_1^2}{2g}, \qquad \dot{W}\left(V_1\right) = \rho \frac{V_1^3}{2} BH\theta_4, \qquad \theta_4 = K \sum_{i=1}^{\infty} \frac{\alpha\beta_i}{i+1} \tag{51}$$

Finally, repeating the procedures for the flow in the region of V_{up}, the power consumption is given by:

$$h_{loss} = K \frac{1}{2g} \left(\frac{H}{\Delta t_y} \right)_{up}^2 = \frac{K}{4\theta_2^2} H, \qquad \dot{W}\left(V_{up}\right) = \rho g V_1 B H^2 \theta_5, \qquad \theta_5 = \frac{K}{4\theta_2^2} \sum_{i=1}^{\infty} \frac{\alpha\beta_i}{i+1} \tag{52}$$

iii. Final equation for CV1 using the results of the global and intrinsic analyses

From equations (38), (41), and (50 to 52), it follows that:

$$g L_r \left(\frac{H}{\Delta t_y} \right)_{up} = \left(\frac{2\theta_3 + 2\theta_5 - 1}{\theta_1} \right) g V_1 H + \frac{\theta_4}{\theta_1} V_1^3 \tag{53}$$

Equations (46) and (53) finally produce:

$$g^{3/2} H^{1/2} L_r = \theta_6 g V_1 H + \theta_7 V_1^3, \quad \text{with} \quad \theta_6 = \sqrt{2}\,\theta_2 \left(\frac{2\theta_3 + 2\theta_5 - 1}{\theta_1} \right) \quad \text{and} \quad \theta_7 = \frac{\sqrt{2}\,\theta_2 \theta_4}{\theta_1} \tag{54}$$

Nondimensional forms for the length L_r obtained from equations (54) are furnished below.

$$\frac{L_r}{H} = \theta_6 Fr_1 \sqrt{h^*} + \theta_7 \left(Fr_1 \sqrt{h^*} \right)^3 \tag{55}$$

http://dx.doi.org/10.5772/58963

$$\frac{L_r}{H} = \theta_6 Fr_H + \theta_7 Fr_H^3 \tag{56}$$

$$\frac{L_r}{h_1} = \theta_6 \frac{Fr_1}{\sqrt{h^*}} + \theta_7 \left(Fr_1\right)^3 \sqrt{h^*} \tag{57}$$

$$\frac{L_r}{h_2} = \theta_6 \frac{Fr_1}{h^{\#}\sqrt{h^*}} + \theta_7 \frac{Fr_1^3 \sqrt{h^*}}{h^{\#}} \tag{58}$$

In equations (55-58), $Fr_H=V_1/(gH)^{1/2}$, and $h^*=h_1/H$. As can be seen, the set of coefficients generated during the global and intrinsic analyses were reduced to only two, θ_6 and θ_7, which must be adjusted using experimental data. The normalizations (57) and (58) showed to be the most adequate for the experimental data analysed here.

2.1.2. Equation for sequent depths and Froude number using control volume 2 (CV2)

It remains to obtain an equation for the sequent depths. CV2 is now used in the stationary flow under study, as shown in Figure 9.

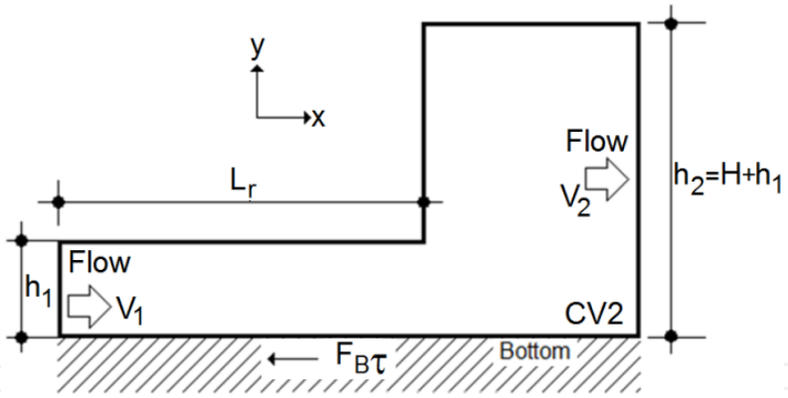

Figure 9. Control volume CV2 used to obtain an equation for the sequent depths.

The forces on CV2 in the contact surfaces between CV1 and CV2 vanish mutually (equilibrium of CV1), thus they are not indicated in Figure 9. In this case, two situations may be considered:

i. The force at the bottom ($F_{B\tau}$) is neglected.

ii. The force at the bottom is relevant.

The solutions in the sequence consider both cases.

i. The force at the bottom is neglected

From the mass conservation equation it follows that:

$$V_2 = V_1 / h^{\#} \tag{59}$$

From the momentum equation it follows that:

$$F_{B_\tau} = \rho B\left(h_2 - h_1\right)[V_1^2 / h^{\#} - g\left(h_1 + h_2\right)/2] \tag{60}$$

Assuming $F_{B\tau}$=0, equation (7) is reproduced, that is:

$$h^{\#} = \left(\sqrt{1+8Fr_1^2} - 1\right)/2 \tag{61}$$

Using h_1 as reference depth (for normalization procedures) equations (57) and (61) form the set of equations that relate the "sizes" h_1, h_2, and L_r in this study. Because $F_{B\tau}$=0, dissipation concentrates in the roller region (CV1). It is of course known that the forces at the interface between both volumes dissipate energy in CV2, but because the momentum equation already furnishes a prediction for h_2/h_1, it is not necessary to use the energy equation for this purpose. On the other hand, when considering the resistive force at the bottom, power losses must be considered in order to obtain predictions for $h^{\#}$.

ii. The force at the bottom is relevant

In this case, from the energy equation it follows that:

$$-\dot{W} = \rho B V_1 h_1 \left(h_2 - h_1\right)\left(g - \frac{V_1^2}{h_2^2}\frac{\left(h_1 + h_2\right)}{2}\right) \tag{62}$$

The left side of equation (62) must consider the power transferred to CV1, denoted by $\dot{W}_{VC1}$, and the power lost due to the shear with bottom of the flow, denoted by $\dot{W}_{FB\tau}$. In mathematical form:

$$\dot{W} = \dot{W}_{VC1} + \dot{W}_{FB\tau} \tag{63}$$

From equations (41), (50), (51) and (52) it follows that:

$$\dot{W}_{VC1} = \rho B V_1 \left(h_2 - h_1\right)[g\left(h_2 - h_1\right)\left(\theta_3 + \theta_5\right) + V_1^2\theta_4 / 2] \tag{64}$$

The velocity close to the bottom is ideally V_1. However, because of the expansion of the flow, it does not hold for the whole distance along the bottom. To better consider this variation, the power loss at the bottom was then quantified using a coefficient θ_8 for V_1, in the form:

http://dx.doi.org/10.5772/58963

$$\dot{W}_{FB\tau} = \theta_8 V_1 F_{B\tau} = \theta_8 V_1 \left\{ \rho B \left(h_2 - h_1 \right) [V_1^2 / h^{\#} - g \left(h_1 + h_2 \right) / 2] \right\} \tag{65}$$

Equations (61) to (65) produce the cubic equation:

$$\left[2\left(\theta_3 + \theta_5 \right) - \theta_8 \right] h^{\#3} + \left[2 - \theta_8 - 2\left(\theta_3 + \theta_5 \right) + \theta_4 Fr_1^2 \right] h^{\#2} - Fr_1^2 \left(1 - 2\theta_8 \right) h^{\#} - Fr_1^2 = 0 \tag{66}$$

The solution of the cubic equation (66) furnishes $h^{\#}$ as a function of Fr_1. Equations (57) and (66) form now the set of equations that relate h_1, h_2, Fr_1, and L_r for power dissipation occurring also in CV2. In section 3 of this chapter, equation (66) **is reduced to a second order equation**, based on the constancy of one of its solutions. Experimental results are then used to test the proposed equations.

The use of the power dissipation introduced coefficients in the obtained equations that affect all parcels having powers of h^* and $h^{\#}$. In order to adjust numerical values to θ_4, θ_8 and $2(\theta_3+\theta_5)$, the following form of equation (66) can be used in a multilinear analysis:

$$Fr_1^2 \left(1 + h^{\#} \right) - 2h^{\#2} = \theta_8 \left[2Fr_1^2 h^{\#} - h^{\#2} \left(1 + h^{\#} \right) \right] + 2\left(\theta_3 + \theta_5 \right) h^{\#2} \left(h^{\#} - 1 \right) + Fr_1^2 h^{\#2} \theta_4 \tag{67}$$

Because multilinear analyses depend on the distribution of the measured values (deviations or errors), different arrangements of the multiplying factors (for example, equations (67) and (68)) may generate different numerical values for θ_4, θ_8 and $2(\theta_3+\theta_5)$.

$$\frac{Fr_1^2 \left(1 + h^{\#} \right) - 2h^{\#2}}{Fr_1^2 h^{\#2}} = \theta_8 \left[\frac{2Fr_1^2 h^{\#} - h^{\#2} \left(1 + h^{\#} \right)}{Fr_1^2 h^{\#2}} \right] + 2\left(\theta_3 + \theta_5 \right) \frac{h^{\#2} \left(h^{\#} - 1 \right)}{Fr_1^2 h^{\#2}} + \theta_4 \tag{68}$$

2.2. Criteria for the function $h(x)$

2.2.1. The "depth deficit" criterion

The focus of the present section is the form of the surface (its profile). Some general characteristics of classical hydraulic jumps were considered, in order to develop a simple criterion, as follows:

i. The mean water depth tends to h_2 downstream from the toe of the jump.

ii. The mean slope of the surface is greater for greater "depth deficits", or differences between h_2 and the local mean water depth h (no undulating surfaces are presently considered).

iii. At the toe, the depth is h_1.

Using x as the longitudinal direction pointing downstream and with origin at the toe of the jump, the second characteristic described above (ii) is expressed mathematically as:

$$\frac{d\,h}{d\,x}\alpha\left(h_2-h\right) \qquad \text{or} \qquad \frac{d\,h}{d\,x}=\theta_{11}\left(h_2-h\right) \tag{69}$$

θ_{11} is a proportionality coefficient with dimension of m^{-1}. The integration of equation (69) using characteristics i and iii as boundary conditions produces:

$$\frac{h-h_1}{h_2-h_1}=1-e^{-\theta_{11}x} \qquad \left(\text{we define } \Pi=\frac{h-h_1}{h_2-h_1} \text{ for further calculations}\right) \tag{70}$$

The surface tends asymptotically to h_2 following an exponential function. The proportionality coefficient must be obtained from experimental data, which is done in section 3. Equation (70) is adequate for surface evolutions without inflexion points.

2.2.2. The "air inflow" criterion

[28] and [29] studied the transition from "black water" to "white water" in spillways and proposed that, if the slope of the surface is produced by the air entrainment, the transfer of air to the water may be expressed in the form:

$$\dot{c}=Kq\frac{d\,h}{d\,x} \tag{71}$$

$\dot{c}$ [s^{-1}] is the air transfer rate (void generation), q [m^2s^{-1}] is the specific water flow rate, h [m] is the total depth of the air-water flow, x [m] is the longitudinal axis and K [m^{-2}] is a proportionality factor. Equation (71) states that higher depth gradients for the same flow rate imply more air entraining the water, the same occurring for a constant depth gradient and higher flow rates. [30] showed that this equation allows obtaining proper forms of the air-water interfaces in surface aeration (stepped spillways).

Considering hydraulic jumps and a 1D formulation, an "ideal" two-step "expansion" of the flow is followed: 1) the flow, initially at velocity V_1 and depth h_1, aerates accordingly equation (71), expanding to ~h_2 ("close" to h_2); 2) the flow loses the absorbed air bubbles, decelerating to V_2 and attaining h_2. The geometrical situation considered in this first analysis is shown in Figure 10.

The evolution of the surface in the first step is obtained using the mass conservation equation:

$$\frac{\partial C}{\partial t}+u\frac{\partial C}{\partial x}+v\frac{\partial C}{\partial y}+w\frac{\partial C}{\partial z}=\left[\frac{\partial}{\partial x}\left(D_T\frac{\partial C}{\partial x}\right)+\frac{\partial}{\partial y}\left(D_T\frac{\partial C}{\partial y}\right)+\frac{\partial}{\partial z}\left(D_T\frac{\partial C}{\partial z}\right)\right]+\dot{p} \tag{72}$$

http://dx.doi.org/10.5772/58963

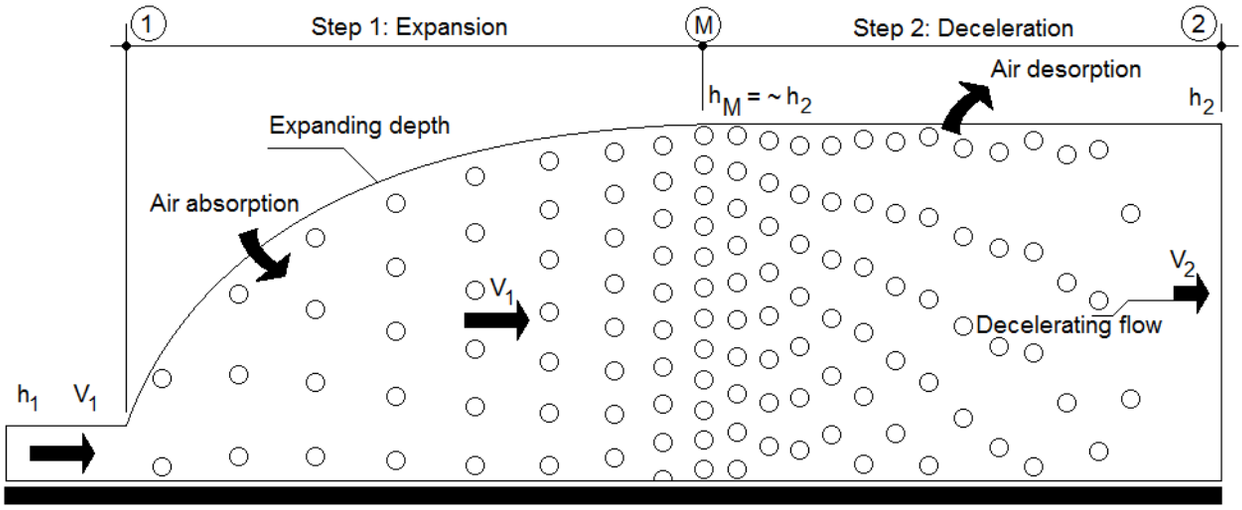

Figure 10. Geometrical condition of this analysis. 1D formulation. Please see also Figure 2.

C is the air concentration in the mixture. u, v, and w, are the velocities along x, y, and z, respectively. D_T is the turbulent diffusivity of the mixture (assumed constant), and $\dot{p}$ is the source/sink parcel. The stationary 1D equation simplifies to:

$$u\frac{\partial C}{\partial x} = D_T\frac{\partial^2 C}{\partial x^2} + \dot{p} \tag{73}$$

Equation (73) is normalized using the density of the air ρ_{air} (the void ratio ϕ is defined as ϕ=C/ρ_{air}), and the length of the jump, L_j, or roller, L_r. Thus we use here simply L (defining s=x/L). The result is:

$$\frac{\partial \phi}{\partial s} = \frac{D_T}{u\,L}\frac{\partial^2 C}{\partial s^2} + \dot{\phi} \tag{74}$$

By normalizing equation (71) to obtain ϕ, the mass discharge of the liquid, $\dot{m}$, was used, so that:

$$\phi = \frac{K\,\dot{m}}{L}\frac{d\,h}{d\,s} \tag{75}$$

K was adjusted to K'. In the 1D formulation the mixture is homogeneous in the cross section. The mean water content in the mixture is expressed as ϕ_{water}=h_1/h. h_1 is the supercritical depth and h=h_1+Z, being h the total depth and Z the length of the air column in the mixture. ρ_{air}<<ρ_{water}, so that:

$$\rho_1/\rho_M = h_M/h_1\ , \qquad \phi = Z/h, \qquad h=h_1/(1-\phi) \tag{76}$$

The indexes 1 and *M* represent the two sections of the flow shown in Figure 10, and ρ is the water density. The integral mass conservation equation furnishes:

$$\dot{m} = \rho_1 h_1 V_1 = \rho_M h_M V_M \qquad \text{or} \qquad V_1 = V_M = u \tag{77}$$

From equations (74) to (77) it follows:

$$\frac{\partial \phi}{\partial s} = \frac{D_T}{V_1 L}\frac{\partial^2 \phi}{\partial s^2} + \frac{K'\dot{m}h_1}{L}\frac{\partial (1-\phi)^{-1}}{\partial s} \tag{78}$$

K´ is a factor that may vary along the flow, and indicates the "facility" of the air absorption by the water. Considering arguments about diffusion of turbulence from the bottom to the surface, [30] proposed $K'=K''h^{-2}$. Equation (79) is then obtained:

$$\frac{\partial \phi}{\partial s} = \omega_1 \frac{\partial^2 \phi}{\partial s^2} + \omega_2 \frac{\partial \phi}{\partial s}, \qquad \text{where} \qquad \omega_1 = \frac{D_T}{V_1 L}, \qquad \omega_2 = \frac{K''\dot{m}h_1}{L} \tag{79}$$

The solution of equation (79), using boundary conditions 1) s=0, ϕ = 0, and 2) $s \to \infty$, $\phi \to \phi_\infty$, and defining $IJ=(\omega_2-1)/\omega_1$, is given by:

$$\phi = \phi_\infty \left(1 - e^{-IJs}\right) \tag{80}$$

Equations (76) and (80) produce:

$$h/h_1 = 1/[1-\phi_\infty(1-e^{-IJs})] \tag{81}$$

In order to obtain a nondimensional depth like equation (70), a boundary layer analogy was followed assuming that at s=1 (length of the roller) we have $h/h_1=\beta h^{\#}$, where β is a constant "close" to the unity (as information, β=0.99 is the boundary layer value, but it does not imply its use here). For $s \to \infty$ we have $h/h_1=h^{\#}$. This implies that $\varphi_\infty=(h^{\#}-1)/h^{\#}$, so that the solution is given now by:

$$\Pi = \frac{h-h_1}{h_2-h_1} = \frac{(1-e^{-IJs})}{h^{\#}-(h^{\#}-1)(1-e^{-IJs})} \qquad IJ = -\ln\left[\frac{1-\beta}{\beta(h^{\#}-1)}\right] \tag{82}$$

http://dx.doi.org/10.5772/58963

Equation (82) is adequate for surface profiles with inflexion points.

2.3. The Random Square Waves rms criterion

The obtained mean profiles of the surface are useful to obtain the profile of the maximum fluctuations of the surface, which may be used in the design of the lateral walls that confine the hydraulic jump. In this sense, the method of Random Square Waves (RSW) for the analysis of random records is used here. Details of this method, applied to interfacial mass transfer, are found in [31, 32]. A more practical explanation is perhaps found in [33], where the authors present the rms function of random records, that is, the "equivalent" to the standard error function (RSW are bimodal records, but used to obtain approximate solutions for general random data).

Equations (70) and (82) express the normalized mean depth h along the hydraulic jump. The RSW approximation considers the maximum (H_2) and minimum (H_1) values of h, that is, it involves the local maxima of the fluctuations. Following the RSW method, the depth profile may be expressed as:

$$\frac{h-H_1}{H_2-H_1}=n \tag{83}$$

The normalized RSW rms function (a "measure" of the standard error) of the depth fluctuations is:

$$\frac{h'}{H_2-H_1}=\sqrt{n(1-n)}\,(1-\alpha) \tag{84}$$

h' is the rms value, and α is called "reduction function", usually dependent on x. From its definition it is known that $0\leq\alpha\leq1$ (see, for example, [33]). [31] and [32] present several analyses using a constant α value, a procedure also followed here as a first approximation. Undulating mean surface profiles, however, need a more detailed analysis.

Equations (70) and (82) to (84) allows obtaining equations for the height attained by fluctuations like waves and drops along the hydraulic jump, using procedures similar to those of normal distributions of random data. For normal distribution of data, 68.2%, 95.5% or 99.6% of the observed events may be computed by using respectively, 1, 2 or 3 standard errors in the prediction (for example). Figure 11 illustrates the comments, where μ represents the mean value and σ represents the standard error. The RSW method uses modified bimodal records (thus, the mentioned percentages may not apply), but the general idea of summing the mean depth and multiples of the rms value is still valid.

In order to relate n from equations (83) and (84) to Π from equations (70) and (82) it was considered that H_1 is zero (no fluctuation crosses the bottom), H_2 is given by $H_2=h_2+Nh_2'$(mean depth summed to N times the rms value), and $h_{wall}=h+Mh'$. Algebraic operations lead to:

$$\frac{h'}{h_2-h_1}=(1-\alpha)\sqrt{\left(\Pi+\frac{1}{h^{\#}-1}\right)\left(1-\Pi+\frac{N^2(1-\alpha)^2h^{\#}}{h^{\#}-1}\right)} \tag{85}$$

$$\frac{h_{wall}}{h_2}=\frac{1}{h^{\#}}+\left(1-\frac{1}{h^{\#}}\right)\left\{\Pi+M(1-\alpha)\sqrt{\left(\Pi+\frac{1}{h^{\#}-1}\right)\left(1-\Pi+\frac{N^2(1-\alpha)^2h^{\#}}{h^{\#}-1}\right)}\right\} \tag{86}$$

h_{wall} is used here to represent the mean height attained by the fluctuations. N and M are constants multiplied by the rms value ("replacing" the standard error) which originally expresses the percentage of cases assumed in the solution. In the present study (1-α) is taken as an adjustment coefficient. When analyzing the maximum value of h_2, the term between braces in equation (86) is substituted by J(max).

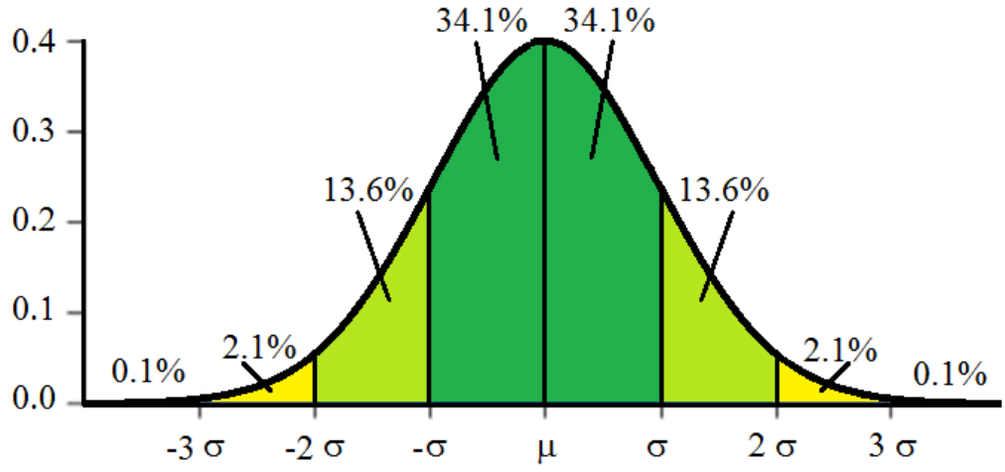

Figure 11. Normal curve showing the percentage of observed cases as the area limited by the curve.

3. Data analyses

3.1. Length of the roller

The data of [18] were first used to test equations (55-58). Different normalizations lead to different adjusted coefficients, because of the different distributions of errors. It was observed here that equation (57) shows the best adjustment to measured data, furnishing the coefficients shown in equation (87), and the adjustment of Figure 12. The obtained correlation coefficient was 0.996. L is used without index (r or j) because both lengths (roller and jet) are used in the following analyses.

http://dx.doi.org/10.5772/58963

$$\frac{L}{h_1} = 3.62\frac{Fr_1}{\sqrt{h*}} - 0.157\left(Fr_1\right)^3\sqrt{h*} \tag{87}$$

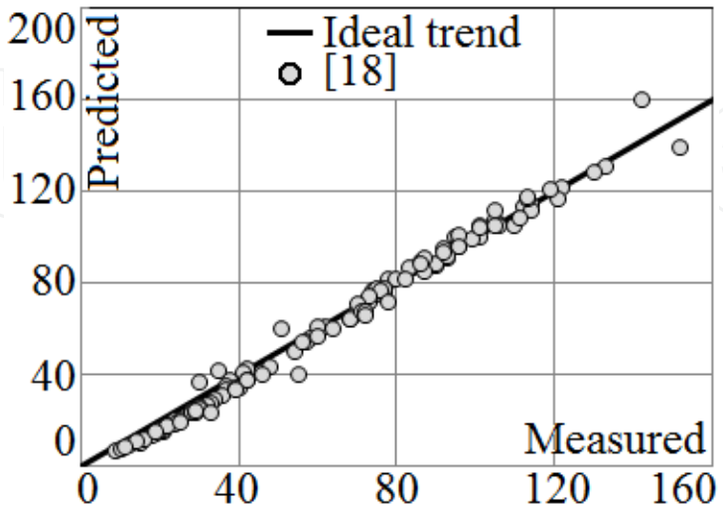

Figure 12. Adjustment of the data of [18] to equation (87).

Having obtained this first adjustment, other data of the literature were also compared to the formulation, obtaining the coefficients of Table 4 (R^2 are those of the multilinear regression). Figure 13 shows all predictions using equation (57) plotted against the measured value. The good linear correlation between predicted and measured values shows the adequacy of the present formulation. Further, different experimental arrangements and definitions of relevant parameters influence the coefficients θ_6 and θ_7, allowing the study of these influences. For the purposes of this study, which intends to expose the adequacy of the formulation, the literature data were used without distinguishing L_r and L_j, or the different ways used to obtain these lengths. Other influences, as the growing of the boundary layer at the supercritical flow, width of the channel, bottom roughness, bottom slope, distance to the downstream control (gate or step), use of sluice gates or spillways at the supercritical flow, among other characteristics, may also be studied in order to establish the dependence of θ_6 and θ_7 on these variables.

Table 4 shows that the coefficients depend on the experimental conditions. As an example, the data of [36] were obtained for several bed slopes. Table 4 presents the coefficients obtained for the slopes of 1° and 5°, suggesting variations in θ_6 and θ_7 (the component of the weight along the channel may influence, for example). Further, the data of [37] were obtained for rough beds, which coefficients may be compared to those for smooth beds of [38], suggesting that roughness also affects the coefficients ([38] also presents data for rough beds, allowing further comparisons). The data of [17] were obtained for flumes having as inlet structure a sluice gate or a spillway, which may be the cause of the different coefficients. The number of "points" of the different series is also shown, in order to allow verifying if the results depend on the "length" of the sample. Because coefficients are adjusted statistically, variations in θ_6 and θ_7 are expected when using only parts of a whole sample (like the two series of [18]). But also

similar results were obtained for data of different authors, like [2], for 17.5º, and [17], for spillways, who furnished samples for 35 and 10 "points", respectively.

Author	θ_6	θ_7	R^2	Number of points
[18] Flume F	5.87	-0.586	0.991	22
[18] All data	3.62	-0.157	0.996	120
[34]	4.13	-0.157	0.995	30
[35]	5.10	-0.373	0.998	50
[2] 16.5ºC	3,43	-0,191	0,999	17
[2] 17.5ºC	2,75	-0,103	0,995	35
[36] 1º Bed slope	4,01	-0,177	0,9998	20
[36] 5º Bed slope	4,30	-0,339	0,9996	14
[37] Data for rough beds	2.76	-0.126	0.998	11
[38] Data for smooth beds	3.60	-0.139	0.994	20
[39]	2.81	-0.187	0.989	72
[15]	4.10	-0.312	0.999	6
[40]	4.65	-0.288	0.9994	31
[17] Spillways	2,79	-0.109	0.9999	10
[17] Sluice gates	2.94	-0.156	0.9999	8

Table 4. Values of θ_6 and θ_7 adjusted to data of different authors.

It is of course necessary to have a common definition of the lengths of the roller and the hydraulic jump (for the different studies) in order to allow a definitive comparison. Historically, different ways to obtain the lengths were used, which may add uncertainties to this first discussion of the coefficients. However, the good joint behavior of the different sets of data shown in Figure 13 emphasizes that such discussion is welcomed.

3.2. Sequent depths for the hypothesis "The force at the bottom is neglected"

Figure 3 already shows the good adjustment obtained using data of different authors. Different conditions of the channel may affect the predictions of equation (7) or (61), as shown in the literature, but the ratio between sequent depths, if working with the classical jump, is well predicted, as can be seen in Figure 3.

3.3. Sequent depths for the hypothesis "The force at the bottom is relevant"

The condition of "not-negligible bottom force" may be relevant, for example, for rough beds, which may affect the length of the jump and the subcritical depth. In order to illustrate this

http://dx.doi.org/10.5772/58963

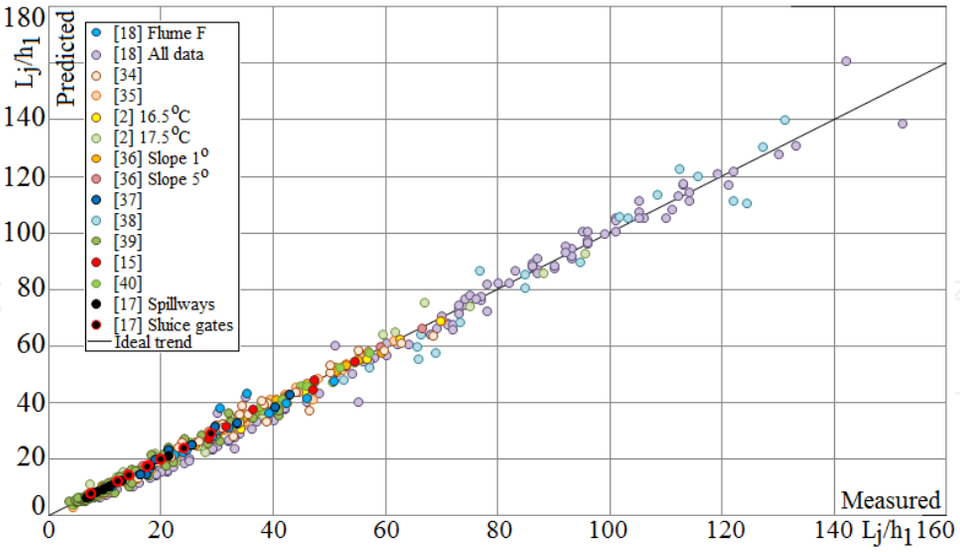

Figure 13. The predictions of L/h_1 for different experiments described in the literatures using the coefficients of Table 4 and equation (57).

condition, a multilinear regression analysis was made using equation (67) and the data of [37], furnishing θ_4=0.001229, θ_8=0.4227, and 2(θ_3+θ_5)=0.5667. The determinant of equation (66) was negative for 10 experimental conditions. Thus, three real roots were obtained for these conditions. On the other hand, the determinant was positive for one experimental condition, leading to only one real root. When plotting the three calculated roots for $h^{\#}$ in relation to the measured values, Figure 14 was obtained (several points superpose).

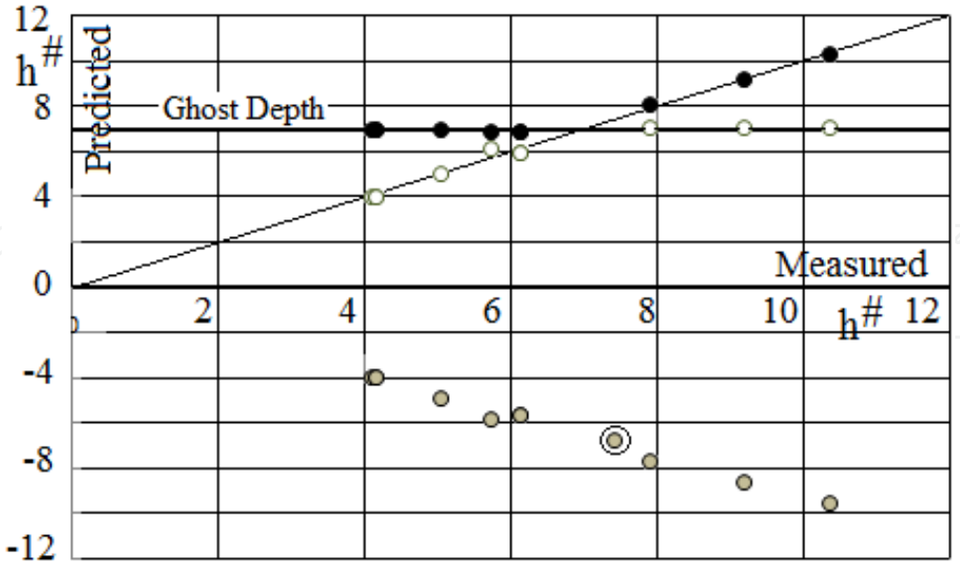

Figure 14. The three roots of $h^{\#}$ predicted with the cubic equation (66) for each experimental condition of [37]. The negative roots (in gray) are physically impossible. The positive roots (in white and black) show a constant depth ratio (Ghost Depth) and the reproduction of the observed values (inclined line). The gray point with a circle corresponds to the real root obtained for the positive determinant of equation (66). Several points superpose.

The constant $h^{\#}$ indicated by the horizontal line was obtained for the different sets of data analyzed here, assuming a proper value for each set. However, because it does not represent an observed result, it was named here "Ghost Depth", h_{GHOST}. From equation (66) this root is quantified as:

$$h_{GHOST} = -\frac{2-\theta_8-2(\theta_3+\theta_5)}{2(\theta_3+\theta_5)-\theta_8} = \frac{(1-2\theta_8)\pm\sqrt{(1-2\theta_8)^2+4\theta_4}}{2\theta_4} \tag{88}$$

Considering the first equality of equation (88), and dividing the cubic equation (66) by the monomial obtained with this solution, following second degree equation is obtained:

$$h^{\#2} - 2\theta_9 Fr_1^2 h^{\#} - \theta_{10} Fr_1^2 = 0 \tag{89}$$

Where:

$$\theta_9 = -\frac{\theta_4}{2[2(\theta_3+\theta_5)-\theta_8]}, \qquad \theta_{10} = \left\{\frac{(1-2\theta_8)}{2(\theta_3+\theta_5)-\theta_8} + \frac{\theta_4[2-\theta_8-2(\theta_3+\theta_5)]}{[2(\theta_3+\theta_5)-\theta_8]^2}\right\}$$

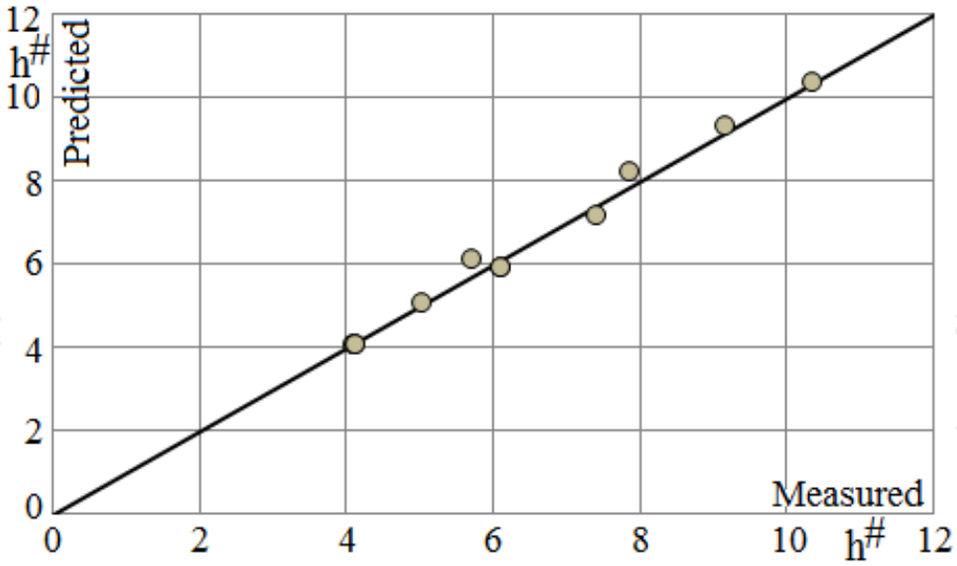

Figure 15. Calculated values of $h^{\#}$ obtained with equation (90) and the data of [37]. The number of experimental conditions is 11, but several points superpose.

As can be seen, also in this case the final equation is a second order equation and depends on only two coefficients, θ_9 and θ_{10}. The solution for $h^{\#}$ is given by:

http://dx.doi.org/10.5772/58963

$$h^{\#} = \theta_9 Fr_1^2 \pm \sqrt{\left[\theta_9 Fr_1^2\right]^2 + \theta_{10} Fr_1^2} \tag{90}$$

The adjusted coefficients produced the graph of Figure 15 for the positive root of equation (90) and the data of [37].

The good result of Figure 15 induced to analyze more data of the literature using equations (89) and (90). Table 5 shows the coefficients obtained from multilinear regression analyses applied to the original data, and Figure 16 presents all data plotted together. The values of R^2 in Table 5 are those obtained in the multilinear regression.

Author	θ_9	θ_{10}	$\sqrt{\theta_{10}}$	R^2	Number of points
[18] Flume F	0.0158	1.44	1.20	0.9993	22
[18] All data	0.00908	1.62	1.27	0.98	120
[34]	0.0138	1.51	1.23	0.998	30
[35]	0.0318	1.27	1.13	0.998	50
[2] 16.5°C	0.00630	1.50	1.22	0,9998	17
[2] 17.5°C	-0.00588	1.78	1.33	0,999	35
[36] 1° Bed slope	0.0437	0.786	0.887	0,9998	20
[36] 5° Bed slope	0.0561	1.14	1.07	0,9996	14
[37] Data for rough beds	0.00375	0.982	0.991	0.998	11
[41] Data for smooth beds	-0.00800	2.52	1.59	0.98	20
[38] Data for smooth beds	0.0165	1.14	1.07	0.990	20
[39]	0.0151	1.50	1.22	0.9993	72
[15]	0.00265	1.72	1.31	0.99995	6
[42] Data for rough beds	-0.00634	1.20	1.10	0.9994	8
[43]	0.0122	1.28	1.13	0.998	10
[40]	0.0684	0.524	0.724	0.98	31
[17] Spillways	0.0119	1.78	1.33	0.993	10
[17] Sluice gates	-0.0320	2.36	1.54	0.96	8

Table 5. θ_9 and θ_{10} (and $\sqrt{\theta_{10}}$) adjusted to data of different authors.

The coefficients θ_9 and θ_{10} of Table 5 show that, for most of the cases, $\theta_{10} >> \theta_9$, which implies $h^{\#} = \theta_9 Fr_1^2 + \sqrt{\theta_{10}} Fr_1$ for the usual range of Fr_1. In many cases, the quadratic term of Fr_1 is still much smaller than the linear term. For example, the data of [15], obtained for $4.38 \le Fr_1 \le 9.26$ produce $\theta_9 Fr_1^2 = 0.227$ and $\sqrt{\theta_{10}} Fr_1 = 12.1$ as their highest values. This fact suggests to use simpler forms

of equation (90) like $h^{\#}=\sqrt{\theta}_{10}Fr_1+Constant$ or $h^{\#}=\sqrt{\theta}_{10}Fr_1$. Both forms appear in the literature. The mean value of $\sqrt{\theta}_{10}$ in table 5 is 1.19, showing that the coefficients of Fr_1 stay around the unity. [44], for example, used $h^{\#}=1.047Fr_1+0.5902$, while [37] simply suggested $h^{\#}=Fr_1$ for their data. Equation (8) of the present chapter is a further example.

A very positive aspect of equation (90) is that it is based on the physical principles of conservation of mass, momentum and energy. The simpler forms of the literature follow directly when analyzing the magnitude of the different parcels of the final equation. That is, the simpler forms are in agreement with the conservation principles (being not only convenient results of dimensional analyses).

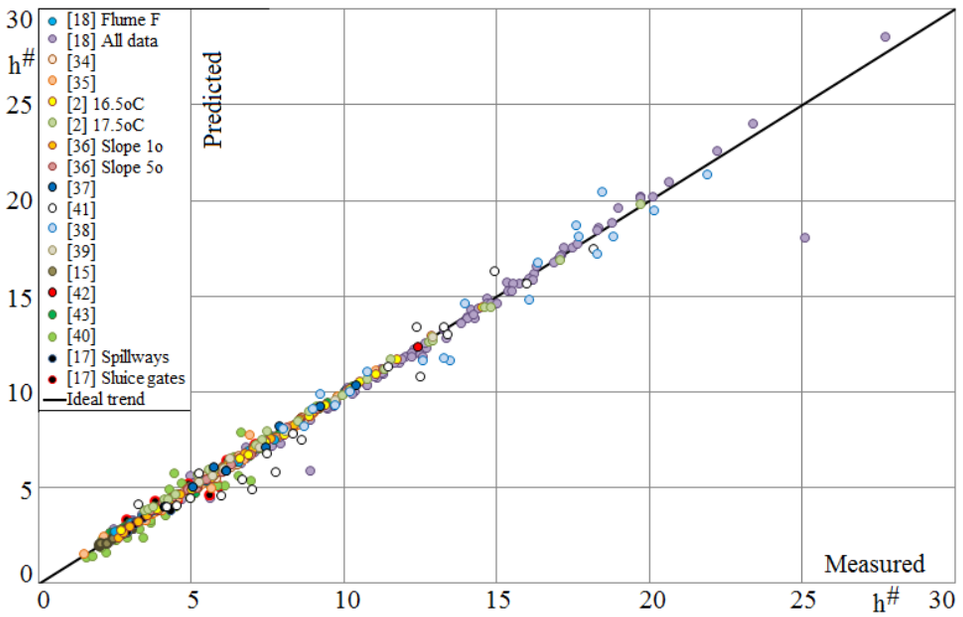

Figure 16. The predictions of h_2/h_1 for different experiments described in the literatures using the coefficients of Table 5 and equation (90).

As an additional information, the coefficient of Fr_1 in the simpler forms tends to be lower than $\sqrt{2}$, the value derived from equations (7) or (61) for no shear force at the bottom of the jump.

From the data analysis performed here, and the conclusions that derive from the presence of the Ghost Depth in the cubic equation, the equations for the geometrical characteristics of hydraulic jumps of case ii of section 2.1.2 (The force at the bottom is relevant) simplify to equation (57) $\frac{L_r}{h_1}=\theta_6\frac{Fr_1}{\sqrt{h^*}}+\theta_7(Fr_1)^3\sqrt{h^*}$ and equation (90) $h^{\#}=\theta_9 Fr_1^2\pm\sqrt{\left[\theta_9 Fr_1^2\right]^2+\theta_{10}Fr_1^2}$, equations already presented in the text.

Considering the deduction procedures followed in this study, the values of θ_6, θ_7, θ_9 and θ_{10} may depend on the factors that determine the resistance forces (shear forces), similarly to the friction factor in uniform flows. Additionally, because $h^*=(h^{\#}-1)^{-1}$, the nondimensional length of the roller may be written as a function only of Fr_1 and the different coefficients.

http://dx.doi.org/10.5772/58963

3.4. Water depth profiles

3.4.1. Profiles without inflexion points

The data of [17] and [25], obtained for spillways, are shown in Figure 17. It is possible to admit no inflexion points in this set of surface profiles. So, equation (70) was used to quantify the surface evolution, furnishing equation (91). The adjustment produced θ_{11}=2.9, implying that x/L=1 (the roller length) is attained for Π=0.95, that is, for 95% of the final depth difference h_2-h_1. Such conditional definition of the length is similar to that used for boundary layer thicknesses, and seems to apply for hydraulic jumps.

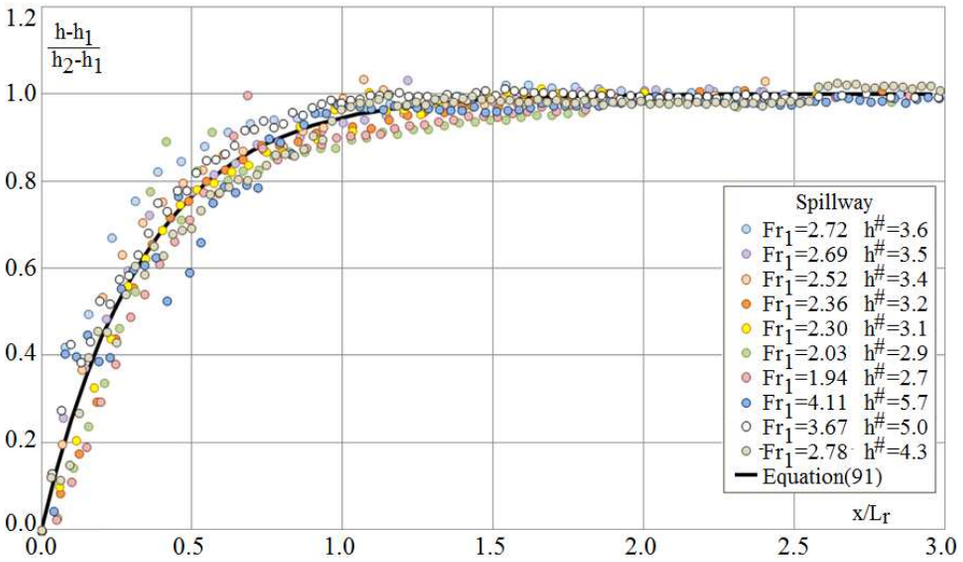

Figure 17. Normalized measured profiles obtained by [17] and [25], adjusted to the exponential prediction (equation 91), for profiles without inflexion points.

In the present analysis, the normalized profile assumes the form

$$\frac{h-h_1}{h_2-h_1}=1-e^{-2.9x/L} \tag{91}$$

3.4.2. Profiles with inflexion points

Equation (82) may be used with any option of $h^{\#}$, that is, equation (61) or (90), or the simpler form $h^{\#}=\sqrt{\theta}_{10}+Constant$. As example, equation (61) is used, generating equation (92) for β=0.99. For comparison, the simpler form of $h^{\#}$ is used (as proposed by [37]) with $\sqrt{\theta}_{10}$=1, *Constant*=0, and β=0.99, resulting $h^{\#}=Fr_1$ and equation (93). Figure 18a shows the comparison between equation (92) and the envelope of the measured data of [37]. Figure 18b shows the comparison between equations (92) and (93) for Fr_1=7. Both equations show the same form, with the results of equation (93) being somewhat greater than those of equation (92).

$$\frac{h-h_1}{h_2-h_1}=\frac{2(1-e^{-IJs})}{(\sqrt{8Fr_1^2+1}-1)-(\sqrt{8Fr_1^2+1}-3)(1-e^{-IJs})} \qquad IJ=-\ln\left[\frac{1}{99(\sqrt{8Fr_1^2+1}-3)}\right] \tag{92}$$

$$\frac{h-h_1}{h_2-h_1}=\frac{(1-e^{-IJs})}{Fr_1-(Fr_1-1)(1-e^{-IJs})} \qquad IJ=-\ln\left[\frac{1}{99(Fr_1-1)}\right] \tag{93}$$

Figure 19 was obtained for the data of [17] using equation (92), but with β=0.97, that is, with the exponent IJ given by:

$$IJ=-\ln\{6/[97(\sqrt{8Fr_1^2+1}-3)]\} \tag{94}$$

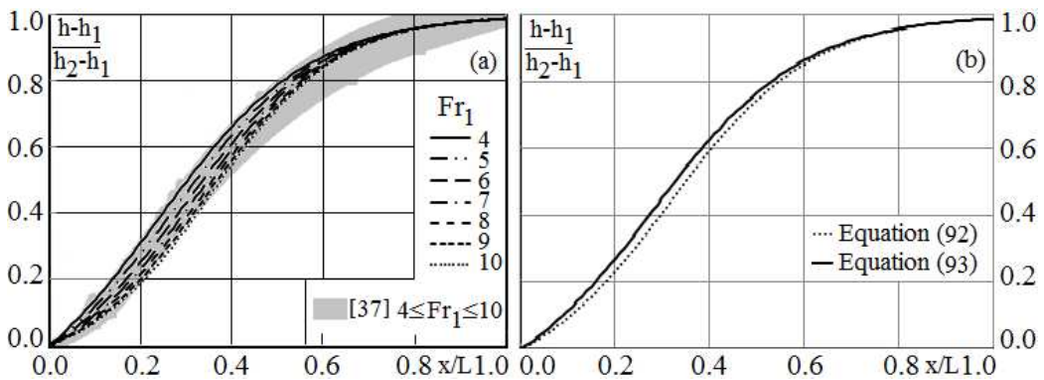

Figure 18. a) The lines are the predictions of equation (92) for the values of Fr_1 shown in the graph (β=0.99). The gray region is the envelope of the data of [37]; b) Comparison between equations (92) and (93) for events with and without bed shear force, and Fr_1=7.0.

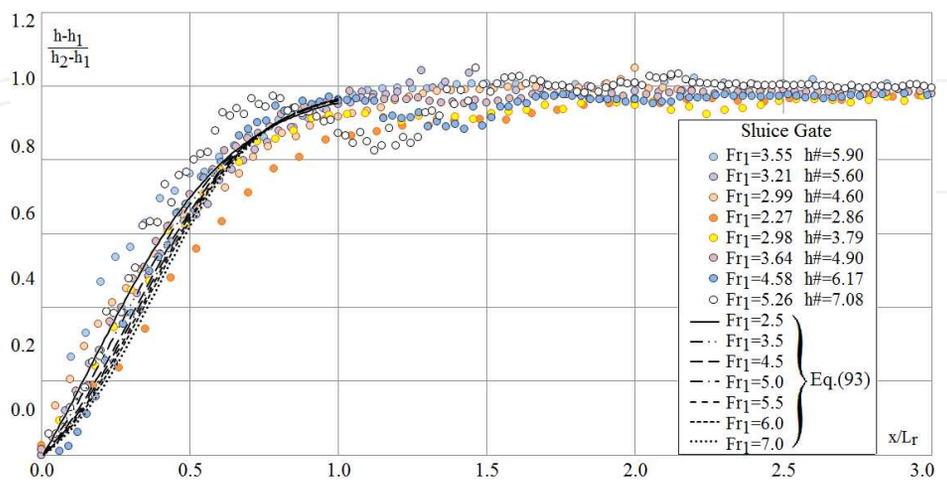

Figure 19. Normalized measured profiles obtained by [17] and [25], and predictions of equation (93) for profiles with inflexion points (β=0.97).

http://dx.doi.org/10.5772/58963

3.4.3. Further normalizations

[21] presented the experimental water profiles shown in Figure 20b. As can be seen, using their normalization the curves intercept each other for the experimental range of Fr_1. In order to verify if the present formulation leads to a similar behavior, a first approximation was made using equation (93) for β=0.95, that is, with the exponent IJ given by

$$IJ = -\ln\{5/[95(Fr_1 - 1)]\}$$

x/L was transformed into $x/(h_2\text{-}h_1)$ by multiplying $[x/(h_2\text{-}h_1)][h_1/L][h^{\#}\text{-}1]$. The coefficients θ_6 and θ_7 of Table 4 for the data of [37] were used to calculate L/h_1, together with $h^{\#}=Fr_1$. The calculated curves shown in Figure 20a also intercept each other, obeying similar relative positions when compared to the experimental curves. The results of the formulation thus follow the general experimental behavior.

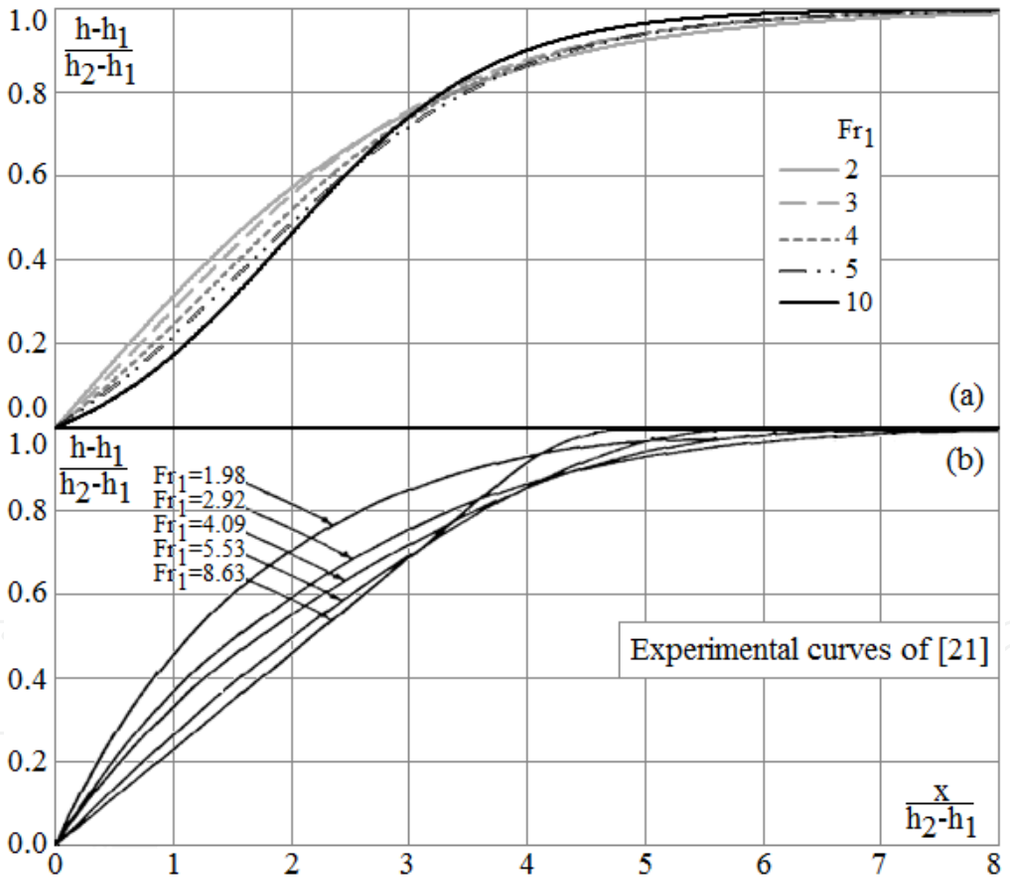

Figure 20. Comparison between observed and calculated surface profiles; a) Calculated curves; b) Experimental curves.

Various values of β were used in the present section (3.4), in order to obtain good adjustments. In each figure (18, 19, and 20) β was maintained constant for the family of curves, but it may not be always the case, considering previous results of the literature. For example, [45]

suggested that the ratio between the final depth of the roller and h_2 is a function or Fr_1. Thus, each curve may have its own β.

3.5. Depth fluctuations and total depths (wall heights)

3.5.1. Predictions based on empirical formulation

As mentioned in item 2.3, oscillations of the free surface may be relevant for the design of side walls. [46] recommended, for the height of the wall, h_{wall}=1.25h_2. [22] performed measurements of water depths and fluctuations along a hydraulic jump in a 40 cm wide horizontal rectangular channel, and imposing Fr_1=3.0. The measurements were made using ultrasonic acoustic sensors. The mean ratio h/h_2 attained a maximum value in the roller region, h_{max}/h_2=1.115. The maximum normalized standard error of the fluctuations along the hydraulic jump was h'_{max}/h_1=0.32 for this condition. [47], based on data of several sources, showed that standard deviation of the fluctuations of the depths in hydraulic jumps increase with the Froude number, suggesting the empirical equation (94), for Fr_1 between 1.98 and 8.5.

$$h'_{max} / h_1 = 0.116(Fr_1 - 1)^{1.235} \tag{95}$$

This equation furnishes, for the condition Fr_1=3.0 studied by [22], the prediction h'_{max}/h_1=0.27, about 16% lower of the experimental value, suggesting further studies. In the present section the height h_{wall} is quantified following different approximations, and using experimental data. A first evaluation of h_{wall} may be given by the sum of the maximum depth and a multiple of the standard deviation (multiple given by the factor N), that is:

$$h_{wall} / h_2 = h_{max} / h_2 + N\, h'_{max} / (h_1 h^{\#}) \tag{96}$$

Using equations (95) and (96), no bed shear force, that is $h^{\#}$=[(1+8Fr_1^2-1)$^{1/2}$-1]/2, and correcting the predicted value of 0.27 to the observed value of 0.32, we have:

$$\frac{h_{wall}}{h_2} = 1.115 + \frac{0.275(Fr_1 - 1)^{1,235}}{\left(\sqrt{1+8Fr_1^2} - 1\right)}, \qquad (N = 1) \tag{97}$$

$$\frac{h_{wall}}{h_2} = 1.115 + \frac{0.550(Fr_1 - 1)^{1,235}}{\left(\sqrt{1+8Fr_1^2} - 1\right)}, \qquad (N = 2) \tag{98}$$

$$\frac{h_{wall}}{h_2} = 1.115 + \frac{0.825(Fr_1 - 1)^{1,235}}{\left(\sqrt{1+8Fr_1^2} - 1\right)}, \qquad (N = 3) \tag{99}$$

http://dx.doi.org/10.5772/58963

As an example, Figure 21 presents different images of surface elevations due to waves, which illustrates a depth fluctuation. Figure 21a presents a sequence of images of a wave passing the hydraulic jump, and Figure 21b shows the relative depth attained by this wave. The approximate value h_{max}/h_2=1.40 is compared with equations (97-99).

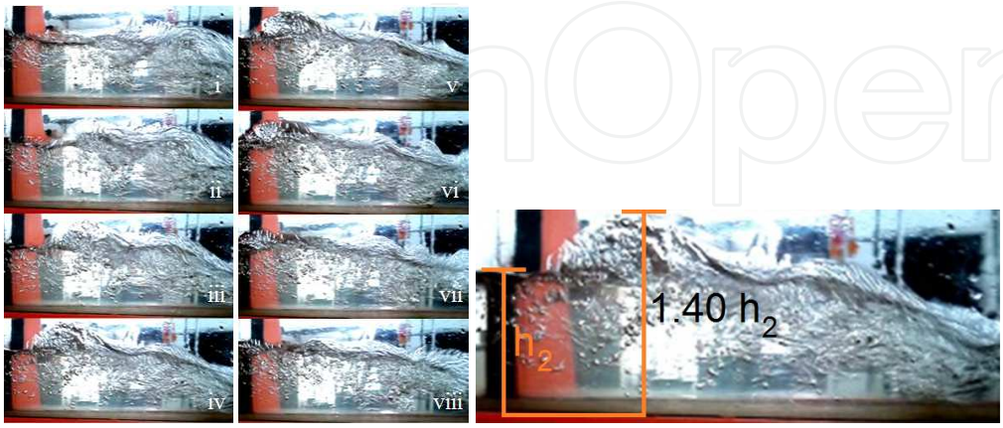

Figure 21. a) Oscillations of the free surface due to a wave in a hydraulic jump for Fr_1=3.5, b) Relative depth attained by the wave shown in Figure 21a iv.

Equations (97, 98, 99) use 1, 2 and 3 standard errors (68.2%, 95.5% and 99.6% of the observed events, respectively, see Figure 13). Figure 22 presents the curves of the three equations, showing that the additional height observed in Figure 21b is better represented by equation (99), for 99.6% of the cases. Equation (97) furnishes values closer to the suggestion of [46] (h_{wall}/h_2=1.25).

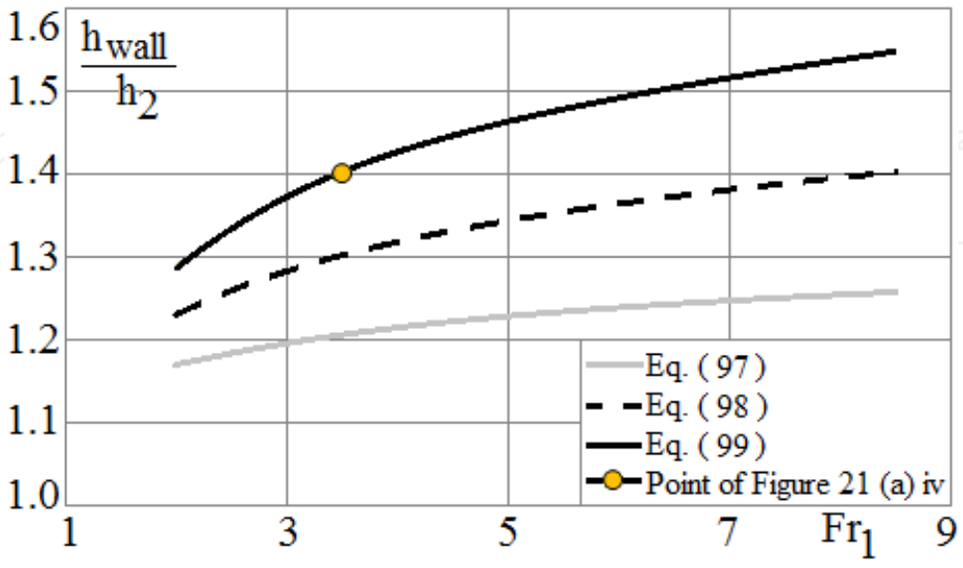

Figure 22. Equations (97, 98, 99), for the maximum depth as a function of the Froude number.

3.5.2. Predictions based on theoretical reasoning

Equations (85, 86) and (91) are used, with N=0.8, M=3.3 and α=0.82. h' and h_{wall} are given by:

$$\frac{h'}{h_2-h_1}=0.18\sqrt{\left(1-e^{-2.9x/L}+\frac{1}{h^{\#}-1}\right)\left(e^{-2.9x/L}+\frac{0.0207h^{\#}}{h^{\#}-1}\right)} \tag{100}$$

$$\frac{h_{wall}}{h_2}=1-\left(\frac{h^{\#}-1}{h^{\#}}\right)e^{-2.9x/L}+0.594\sqrt{\left[1-\left(\frac{h^{\#}-1}{h^{\#}}\right)e^{-2.9x/L}\right]\left[\left(\frac{h^{\#}-1}{h^{\#}}\right)e^{-2.9x/L}+0.0207\right]} \tag{101}$$

Predictions of equation (101) were compared with depth data obtained by [17]. The comparison is shown in Figure 23. The normalized mean depth of the data increases continuously with x/L_r, but when added to three times the standard error, the points show a very slight maximum. For the predictive calculations, it was assumed H_1=0 (a limiting value), but any value $0 \le H_1 \le h_1$ is possible. The value M=3.3 multiplied by the rms function of the RSW method is close to the "three standard error" used for h_{wall}/h_2. For Fr_1=2.36 the maximum calculated value is h_{wall}/h_2=1.11, lower than the suggested value of [46], that is, h_{wall}/h_2=1.25. Figure 24 shows the data measured by [17], where the vertical lines are the measured points.

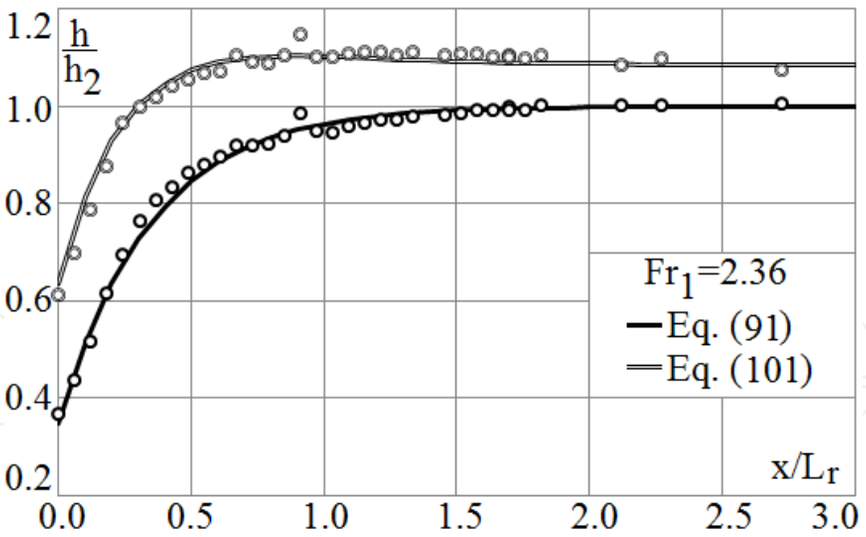

Figure 23. Measured surface profile (lower "o"), and 3 standard errors added to it (upper "o"). Data of [17]. Calculated profile (equation 91) and 3.3 times the rms value of the RWS method added to it (equation 101).

Predictions similar to those presented in Figure 22 need only the maximum value of the function along x/L_r. Indicating this value as "J(max)", equations (101) and (61) furnish, for no bed shear force:

http://dx.doi.org/10.5772/58963

$$\frac{h_{wall}}{h_2}=\frac{2}{\sqrt{1+8Fr_1^2}-1}+\left(\frac{\sqrt{1+8Fr_1^2}-3}{\sqrt{1+8Fr_1^2}-1}\right)J\left(\max_1\right),\qquad \text{adjusted}\quad J(\max_1)=1.515 \tag{102}$$

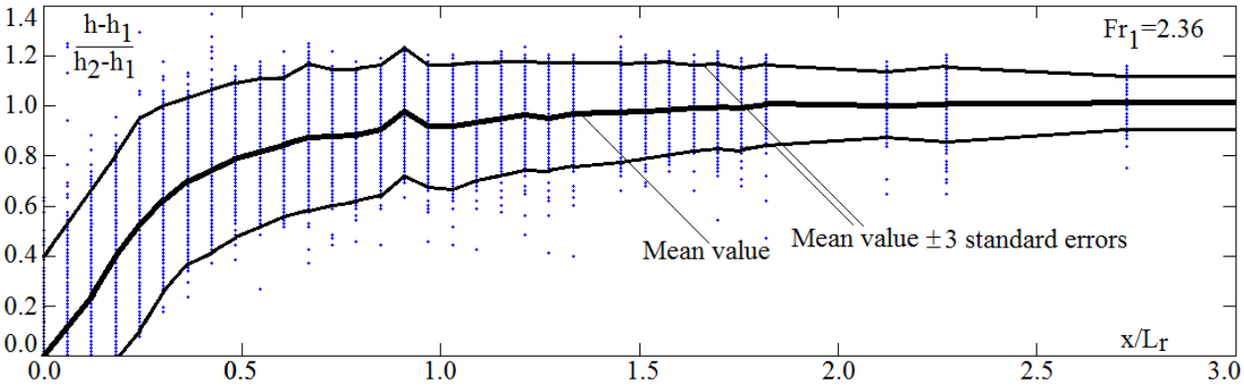

Figure 24. Measurements of [17] used in Figure 23.

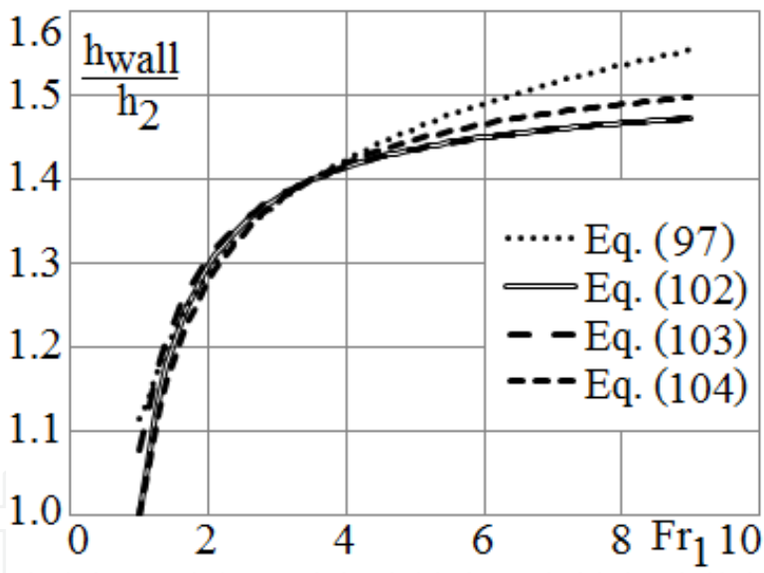

Figure 25. Equations (97), (102), (103) and (104) for the maximum depth as a function of the Froude number. J(max) adjusted for h_{wall}/h_2=1.4 and Fr_1=3.5.

For bed shear forces the form $h^{\#}=\sqrt{\theta}_{10}Fr_1+Constant$ can be used. As example, equation (101) together with equation (8) or $h^{\#}=Fr_1$ (see [37]) furnish, respectively:

$$\frac{h_{wall}}{h_2}=\frac{1}{1.29Fr_1-0.116}+\left(\frac{1.29Fr_1-1.116}{1.29Fr_1-0.116}\right)J\left(\max_2\right),\qquad \text{adjusted}\ J(\max_2)=1.518 \tag{103}$$

$$\frac{h_{wall}}{h_2} = \frac{1}{Fr_1} + \left(\frac{Fr_1 - 1}{Fr_1}\right) J(\max_3), \qquad \text{adjusted } J(\max_3)=1.560 \tag{104}$$

The theoretical predictions of equations (99), (102), (103) and (104) on the Froude number (Fr_1) are shown in Figure 25. J(max) was adjusted in each equation to furnish h_{wall}/h_2=1.4 for Fr_1=3.5. J(max) also corresponds to the maximum value of h_{max}/h_2 for each prediction.

The theoretical predictions of h_{wall}/h_2 follow the general trend obtained when using the empirical approximation of [47], that is, higher h_{wall}/h_2 are obtained for higher Fr_1 (for the observed Fr_1 range). However, the condition h_{wall}/h_2=1.4 for Fr_1=3.5 was observed only in laboratory scale (see Figure 21). Scale-up studies are thus needed.

4. Conclusions

The conclusions are presented as suggestions of use for conditions similar to those of the mentioned experimental studies. The numbers of the equations refer to their location in the text.

4.1. Basic lengths

Condition: No bed resistance (no bed shear forces).

For the length of the roller, use (see Table 4 and Figure 13):

(Applied principles: conservation of mass, momentum, and energy).

Equation (57): $\frac{L_r}{h_1} = \theta_6 \frac{Fr_1}{\sqrt{h^*}} + \theta_7 (Fr_1)^3 \sqrt{h^*}$

For the sequent depths, use (see Figure 3):

(Applied principles: conservation of mass and momentum).

Equation (61): $h^{\#} = \left(\sqrt{1 + 8Fr_1^2} - 1\right)/2$

Condition: Relevant bed resistance (presence of shear forces).

For the length of the roller, use (see Table 4 and Figure 13):

(Applied principles: conservation of mass, momentum, and energy).

Equation (57): $\frac{L_r}{h_1} = \theta_6 \frac{Fr_1}{\sqrt{h^*}} + \theta_7 (Fr_1)^3 \sqrt{h^*}$

For the sequent depths, use (see Table 5 and Figure 16):

(Applied principles: conservation of mass, momentum, and energy).

http://dx.doi.org/10.5772/58963

Equation (90): $h^{\#} = \theta_9 F r_1^2 + \sqrt{\left[\theta_9 F r_1^2\right]^2 + \theta_{10} F r_1^2}$

As shown in the text (see Table 5), the magnitude of the parcels of equation (90) also allows using the simplified forms, linked to the three principles of conservation used in equation (90):

$$h^{\#} = \sqrt{\theta_{10}} F r_1 + \theta_9 F r_1^2$$

$$h^{\#} = \sqrt{\theta_{10}} F r_1 + Constant$$

$$h^{\#} = \sqrt{\theta_{10}} F r_1$$

4.2. Surface evolution (surface profile)

For surfaces without inflexion point, use (see Figure 17):

(Applied "principle": Depth deficit).

Equation (70): $\frac{h - h_1}{h_2 - h_1} = 1 - e^{-\theta_{11}^* x/L}$ with $\theta_{11}^* = L\ \theta_{11}$

The data analyzed in the present study furnished $\theta_{11}^* \approx 2.9$. But the evolution of the surface depends on operation conditions, and more studies are necessary.

For surfaces with inflexion point, use (see Figures 18, 19, 20):

(Applied principles: Conservation of mass (air and water) and basic air transfer equation (void generation).

Equation (82): $\frac{h - h_1}{h_2 - h_1} = \frac{(1 - e^{-IJs})}{h^{\#} - (h^{\#} - 1)(1 - e^{-IJs})}$ with $IJ = -\ln\left[\frac{1 - \beta}{\beta(h^{\#} - 1)}\right]$

The exponential form is maintained in the equation for simplicity.

4.3. Fluctuations and related depths (for lateral walls)

(Applied principle: rms of fluctuations as obtained in the RSW method).

For the dependence with the Froude number Fr_1, use:

Equation (86): $\frac{h_{wall}}{h_2} = \frac{1}{h^{\#}} + \left(1 - \frac{1}{h^{\#}}\right) J(\max)$

From laboratory observations for Fr_1=3.5 (see Figure 21), the value of J(max) in this study varied between 1.52 and 1.56. But scale-up procedures are still necessary. $h^{\#}$ depends on the situation under study: with or without bed shear forces (using the equations for $h^{\#}(Fr_1)$ presented here).

For the evolution of the height attained by fluctuations along the jump, use:

Equation (85): $\frac{h'}{h_2 - h_1} = (1 - \alpha)\sqrt{\left(\Pi + \frac{1}{h^{\#} - 1}\right)\left(1 - \Pi + \frac{N^2 (1 - \alpha)^2 h^{\#}}{h^{\#} - 1}\right)}$

Equation (86): $\frac{h_{wall}}{h_2}=\frac{1}{h^{\#}}+\left(1-\frac{1}{h^{\#}}\right)\left\{\Pi+M(1-\alpha)\sqrt{\left(\Pi+\frac{1}{h^{\#}-1}\right)\left(1-\Pi+\frac{N^2(1-\alpha)^2h^{\#}}{h^{\#}-1}\right)}\right\}$

h_{wall} is used here to represent the mean total height attained by the fluctuations. N and M are constants. In the present study N=0.8 (close to 1, for the equivalent to the standard error), M=3.3 (close to 3, considering more events) and α=0.8 ($0\leq\alpha\leq1$ from the RSW method). Π was represented for a situation without inflexion points, that is, using equation (70) or (91).

4.4. Challenges

Having a set of equations for geometrical aspects of hydraulic jumps, which fit observed characteristics of different experimental situations, following questions need attention:

- Table 4 shows a somewhat broad range of values for coefficients θ_6 and θ_7 (although each of them maintains a coherent magnitude). In this table no distinction was made between the lengths of the roller and the jump itself. Also the different definitions and measurement procedures were not distinguished. A "standard definition" for the roller length and the jump length would help to compare different experimental results. In addition, the influences of experimental conditions on the coefficients may be studied in a systematic way (geometry, size, distribution of roughness elements, slope of the bed, etc., like usual studies of resistance factors or coefficients), which certainly will help the practical use of equation (57).

- Table 5 shows that the coefficients θ_9 and θ_{10} also maintain coherent magnitudes. In this case, $\sqrt{\theta_{10}}$ stays around the unity for the experimental data used here (mean value of 1.19). Also here a systematic study may furnish the dependence of the coefficients on controlled parameters, like roughness and slope. Such study will help the practical use of equation (90) and its simpler forms.

- The form of the surface for the conditions "with inflexion point" and "without inflexion point" was considered here for monotonic growing profiles. The form of the profile is important to detect the end of strong surface variations. In this case, a conditional length may be defined, similarly to the boundary layer thickness. In the present study the values 95%, 97% and 99% of $(h-h_1)/(h_2-h_1)$ were used to define the "roller length" or the "jump length", but it was mentioned that the literature already shows proposals in this sense, which may imply in broader ranges of values. A "standard definition" in this sense, would probably diminish the "imprecisions" of the multiple definitions and measurement strategies found in the literature. Additionally, ultrasound probes and high speed cameras have shown to be adequate to obtain information of the surface evolution, enabling to verify such conditional definitions. Undulating surfaces were not considered in the present study.

- The use of the conclusion $h'/(H_2-H_1)=\sqrt{n(1-n)}(1-\alpha)$ of the RSW method shows that it is possible to have a first prediction of the form of the height attained by the fluctuations along the jump based on the form of the mean surface profile for monotonic growing surfaces. More studies could establish adequate values (or functions) for α for the different experimental conditions, for example.

http://dx.doi.org/10.5772/58963

Author details

Harry Edmar Schulz[1*], Juliana Dorn Nóbrega[1], André Luiz Andrade Simões[2], Henry Schulz[3] and Rodrigo de Melo Porto[1]

*Address all correspondence to: heschulz@sc.usp.br

1 University of São Paulo, Brazil

2 Federal University of Bahia, Brazil

3 Educational Cooperative – Educativa São Carlos, Brazil

References

[1] Elevatorski EA. Hydraulic Energy Dissipators. New York: McGraw-Hill; 1959.

[2] Hager WH, Bremen R, Kawagoshi N. Classical hydraulic jump: length of roller. Journal of Hydraulic Research 1990;28 591-608.

[3] Ortiz JP. Macroturbulência de escoamentos à jusante de estruturas de dissipação por ressalto: estudo teórico-experimental. MSc Thesis. University of São Paulo; 1982.

[4] Ortiz JP. Estrutura e resolução de pressões flutuantes - sua análise randômica na base do ressalto hidráulico. PhD Thesis. University of São Paulo; 1989.

[5] Gil MML. Ressalto hidráulico em pressão a jusante em conduto circular inclinado. MSc Thesis. University of São Paulo; 1991.

[6] Yamashiki Y. Modelação matemática e física da erosão em presença de ressalto hidráulico. MSc Thesis. University of São Paulo; 1994.

[7] Gomes JF. Visualização de escoamento macroturbulento - ressalto hidráulico a jusante de uma comporta. MSc Thesis. Federal University of Rio Grande do Sul; 2000.

[8] Trierweiler Neto EF. Avaliação do campo de pressões em ressalto hidráulico formado a jusante de uma comporta com diferentes graus de submergência. MSc Thesis. Federal University of Rio Grande do Sul; 2006.

[9] Wiest RA. Avaliação do campo de pressões em ressalto hidráulico formado a jusante de um vertedouro com diferentes graus de submergência. MSc Thesis. Federal University of Rio Grande do Sul; 2008.

[10] Alves AAM. Caracterização das solicitações hidrodinâmicas em bacias de dissipação por ressalto hidráulico com baixo número de Froude. MSc Thesis. Federal University of Rio Grande do Sul; 2008.

[11] Quevedo DM. Análise de pressões junto ao fundo no ressalto hidráulico formado a jusante de um vertedouro através da distribuição bivariada de valores extremos. PhD Thesis. Federal University of Rio Grande do Sul; 2008.

[12] Cerezer SM. Uso da teoria de valores extremos para estimar valores de pressões hidrodinâmicas em um ressalto hidráulico formado a jusante de um vertedouro: o caso da UHE Porto Colômbia. PhD Thesis. Federal University of Rio Grande do Sul; 2008.

[13] Teixeira ED. Efeito de escala na previsão dos valores extremos de pressão junto ao fundo em bacias de dissipação por ressalto hidráulico. PhD Thesis. Federal University of Rio Grande do Sul; 2008.

[14] Ortiz JP. Fundamentos da turbulência de escoamentos incompressíveis aplicados à engenharia. Associate Professor Thesis. University of São Paulo; 2011.

[15] Dai Prá M. Uma abordagem para determinação das pressões junto ao fundo de dissipadores de energia por ressalto hidráulico. PhD Thesis. Federal University of Rio Grande do Sul; 2011.

[16] Souza PEA. Bacias de dissipação por ressalto hidráulico com baixo número de Froude - análise das pressões junto ao fundo da estrutura. MSc Thesis. Federal University of Rio Grande do Sul; 2012.

[17] Nóbrega JD. Metodologia teórica e experimental para determinação das características do ressalto hidráulico clássico. MSc Thesis. University of São Paulo; 2014.

[18] Peterka AJ. Hydraulic design of stilling basins and energy dissipators. Engineering Monograph No. 25, 8th ed. United States Department of the Interior, Bureau of Reclamation; 1984.

[19] Marques MG, Drapeau J, Verrette JL. Flutuação de pressão em um ressalto hidráulico. Revista Brasileira de Recursos Hídricos 1997; 2, 45-52.

[20] Hager WH. Energy Dissipators and Hydraulic jump. Water Science and Technology Library, Vol. 8. The Netherlands: Kluwer Academic Publishers; 1992.

[21] Bakhmeteff BA, Matzke AE. The hydraulic jump in terms of dynamic similarity. Transactions of the American Society of Civil Engineers 1936; 101 630-647.

[22] Simões ALA, Schulz HE, Porto RM. Simulação numérica e verificação experimental da posição da superfície livre de um ressalto hidráulico em um canal retangular. In: IAHR, XXIV Congresso Latinoamericano de Hidráulica, November 2010, Punta del Este, Uruguay.

[23] Simões ALA, Porto RM, Schulz HE. Superfície livre de escoamentos turbulentos em canais: vertedores em degraus e ressalto hidráulico. Revista Brasileira de Recursos Hídricos 2012; 17 125-139.

[24] Nóbrega JD, Schulz HE, Simões ALA, Porto RM. Measurement of turbulence parameters in hydraulic jumps using ultrasonic sensors and their correlation with macro-

scopic flow parameters. In: COBEM 2013: 22nd International Congress of Mechanical Engineering, 3-7 November 2013, Ribeirão Preto, Brazil.

[25] Nóbrega JD, Schulz HE, Zhu DZ. Free surface detection in hydraulic jumps through image analysis and ultrasonic sensor measurements. In: Chanson H, Toombes L. (eds.) Hydraulic Structures and Society - Engineering Challenges and Extremes: proceedings of the 5th IAHR International Symposium on Hydraulic Structures, ISHS2014, 25-27 June 2014, Brisbane, Australia.

[26] Simões ALA. Considerações sobre a hidráulica de vertedores em degraus: metodologias adimensionais para pré-dimensionamento. MSc thesis. University of São Paulo; 2008.

[27] Simões ALA, Schulz HE, Porto RM. Stepped and smooth spillways: resistance effects on stilling basin lengths. Journal of Hydraulic Research 2010; 48 329–337.

[28] Schulz HE, Simões ALA. Desenvolvimento da superfície livre em escoamentos aerados: analogia com leis básicas de transferência. Report I/II/11; 2011. Available from: http://stoa.usp.br/hidraulica/files/-1/16207/Schulz_H.E._Simões_A.L.A_LTR-Relatório+I_II_11.pdf (acessed 21 July 2014).

[29] Schulz HE, Simões ALA. Desenvolvimento da superfície livre em escoamentos aerados: analogia com leis básicas de transferência. Revista Brasileira de Recursos Hídricos 2013; 18 35–44.

[30] Schulz HE, Lobosco RJ, Simões ALA. Multiphase analysis of entrained air in skimming flows along stepped chutes. In: Hogge M, Van Keer R, Dick E, Malengier B, Slodicka M, Béchet E, Geuzaine C, Noels, L, Remacle J-F. (eds.) ACOMEN 2011: proceedings of the Fifth International Conference on Advanced Computational Methods in Engineering, 14-17 November 2011, Liège, Belgium. Université Catholique de Louvain/Université de Liège/Universiteit Gent: Leuven.

[31] Schulz HE, Lopes Júnior GB, Simões ALA, Lobosco RJ. One dimensional turbulent transfer using random square waves – scalar/velocity and velocity/velocity interactions. In: Schulz HE, Simões ALA, Lobosco RJ. (eds.) Hydrodynamics – Advanced Topics. 1 ed. InTech; 2011. p3-34.

[32] Schulz HE, Simões ALA, Janzen JG. Statistical approximations in gas-liquid mass transfer. In: Komori S, McGillis W, Kurose R. (eds.) GTWS 2010: proceedings of the 6th International Symposium on Gas Transfer at Water Surfaces 2010, 17-21 May 2010, Kyoto, Japan. Kyoto: Kyoto University Press; 2011.

[33] Schulz HE, Janzen JG. Concentration fields near air-water interfaces during interfacial mass transport: oxygen transport and random square wave analysis. Brazilian Journal of Chemical Engineering 2009; 26 527–536.

[34] Hughes WC, Flack JE. Hydraulic jump properties over a rough bed. Journal of Hydraulic Engineering 1984; 110 1755–1771.

[35] Bhutto HBG. Hydraulic jump control and energy dissipation. PhD thesis. Institute of Irrigation and Drainage Engineering, Mehran University of Engineering and Technology; 1987.

[36] Li C-F. Determining the location of hydraulic jump by model test and HEC-2 flow routing. MSc thesis. College of Engineering and Technology, Ohio University; 1995.

[37] Ead SA, Rajaratnam N. Hydraulic jumps on corrugated beds. Journal of Hydraulic Engineering 2002; 128 656–663.

[38] Evcimen TU. The effect of prismatic roughness elements on hydraulic jump. MSc thesis. The Graduate School of Natural and Applied Sciences, Middle East Technical University; 2005.

[39] Carollo FG, Ferro V, Pampalone V. Hydraulic jumps on rough beds. Journal of Hydraulic Engineering 2007; 133 989–999.

[40] Gandhi S, Yadav V. Characteristics of supercritical flow in rectangular channel. International Journal of Physical Sciences 2013; 8 1934–1943.

[41] Ayanlar K. Hydraulic jump on corrugated beds. MSc thesis. Middle East Technical University; 2004.

[42] Salehian S, Bajestan MS, Jahromi HM, Kashkooli H, Kashefipour SM. Hydraulic jump characteristics due to natural roughness. World Applied Sciences Journal 2011; 13 1005–1011.

[43] Souza PMBM. Estudo da dissipação de energia por ressalto hidráulico a jusante de descarregadores não convencionais. University of Porto; 2011.

[44] Izadjoo F, Bejestan MS. Corrugated bed hydraulic jump stilling basin. Journal of Applied Sciences 2007; 7 1164–1169.

[45] Rajaratnam, N. Hydraulic Jumps, in: Chow, VT. (ed) Advances in Hydroscience v.4, New York: Academic Press; 1967, 197-280.

[46] Lencastre A. Hidráulica Geral. Lisbon: Author Edition; 1996.

[47] Murzyn F, Chanson H. Free-surface fluctuations in hydraulic jumps: experimental observations. Experimental Thermal and Fluid Science 2009; 33 1055–1064.